DMD Fast Forward. Published on February 19, 2013 as doi:10.1124/dmd.112.050450

Contribution of Artifacts to *N*-Methylated Piperazine Cyanide-Adduct Formation *in vitro* from *N*-Alkyl Piperazine Analogs

Minli Zhang, Christina M. Resuello, Jian Guo, Mark E. Powell, Charles S. Elmore, Jun Hu and Karthick Vishwanathan

Drug Metabolism and Pharmacokinetics, AstraZeneca Pharmaceuticals, Boston, MA, USA (M.Z., J.G., K.V.), Medicinal Chemistry, AstraZeneca Pharmaceuticals, Boston, MA, USA (J.H.) and CNS discovery, AstraZeneca Pharmaceuticals, Wilmington, DE, USA (C.M. R., M. E. P., C.S.E.)

Running Title Page

Running Title: Artifacts in *N*-methyl piperazine cyanide-adduct formation

Corresponding author:

Minli Zhang, Ph.D.

Drug Metabolism and Pharmacokinetics

AstraZeneca Pharmaceuticals

35 Gatehouse Dr.

Waltham, USA 02451

Tel 1-781-8394411

Fax 1-781-7425926

Email minli.zhang@AstraZeneca.com

Document Summary:

Number of Text Pages: 15

Number of Tables: 3

Number of Figures: 20

Number of References: 29

Number of Words in the Abstract: 249

Number of Words in the Introduction: 511

Number of Words in the Discussion: 1237

Non-standard abbreviations used are: ESI, Electrospray ionization; HLM, Human liver microsomes; RLM, Rat liver microsomes; ADRs, Adverse drug reactions; MBI, Mechanism-based inactivation; CN-adduct, cyanide-adduct; LC/MS, Liquid chromatography coupled with mass spectrometry; Rt, Retention time; *m/z*, Mass to charge ratio; MS, Mass spectrometry; CE,

collision energy; amu, atomic mass unit(s); NL, Neutral loss; NL-27, Neutral loss of 27 amu; UPLC, Ultra Performance Liquid Chromatography.

DMD Fast Forward. Published on February 19, 2013 as DOI: 10.1124/dmd.112.050450

Abstract

In the liver microsome cyanide trapping assays piperazine containing compounds were found to form significant *N*-methyl piperazine cyanide (CN) adducts. Two pathways for the *N*-methyl piperazine CN-adduct formation were proposed. (1) The α-carbon in the *N*-methyl piperazine is oxidized to form a reactive iminium ion which can react with cyanide ion. (2) *N*-dealkylation occurs followed by condensation with formaldehyde and dehydration to produce *N*-methylenepiperazine iminium ion which then reacts with cyanide ion to form the *N*-methyl CN-adduct. The CN-adduct from the second pathway was believed an artifact or metabonate. In the present study, a group of 4′-*N*-alkyl piperazines and 4′-*N*-[^{13}C]methyl labeled piperazines were used to determine which pathway was predominant. Following microsomal incubations in the presence of cyanide ions, a significant percentage of 4′-*N*-[^{13}C]methyl group in the CN-adduct was replaced by an unlabeled natural methyl group suggesting that the second pathway was predominant. For 4′-*N*-alkyl piperazine, the level of 4′-*N*-methyl piperazine CN-adduct formation was limited by the extent of prior 4′-*N*-dealkylation. In a separate study, when 4′-*NH*-piperaziens were incubated with KCN and [^{13}C]-labeled formaldehyde, 4′-*N*-[^{13}C]methyl piperazine CN-adduct was formed without NADPH or liver microsome suggesting a direct Mannich reaction is involved. However, when [^{13}C]-labeled methanol or potassium carbonate was used as the one-carbon donor, 4′-*N*-[^{13}C]methyl piperazine CN-adduct was not detected without liver microsome or NADPH present. The biological and toxicological implications of bioactivation *via* the second pathway necessitate further investigation because these one-carbon donors for the formation of reactive iminium ions could be endogenous and readily available *in vivo*.

DMD Fast Forward. Published on February 19, 2013 as DOI: 10.1124/dmd.112.050450

Introduction

Drug induced toxicity is one of the major reasons for withdrawal of marketed drugs (Kaplowitz, 2005). Investigation of the underlying mechanisms for adverse drug reactions (ADRs) is among the major efforts of pharmaceutical companies along with managing risks associated with acute toxicities (Smith and Obach, 2009). Drugs that are metabolized to generate electrophilic reactive intermediates which can form covalent adducts with macromolecules carry an increased risk of ADRs or idiosyncratic toxicity (Walgren et al, 2005; Waring, 2005; Ulrich, 2007) and drug-drug interactions caused by mechanism-based inactivation (MBI) of P450 enzymes (Orr et al, 2012). Glutathione (GSH), potassium cyanide (KCN), methoxyamine and semicarbazide have become widely used as trapping agents to evaluate the metabolic activation potential of drug molecules (Evans, 2004; Kalgutkar and Soglia, 2005; Kumar et al, 2008). Cyanide was first introduced as an agent in 1950s to study hard electrophilic molecules such as *N*-substituted nicotinamide compounds (Colowick et al, 1951). Alicyclic amines such as nicotine and prolintane that form hard electrophilic iminium ions, are highly reactive with cyanide, suggesting their potential to react with macromolecules (Murphy, 1973). Other alicyclic amines such nefazodone, indinavir, and prochlorperazine have also been shown to form iminium ions that react with cyanide (Gorrod and Aislaitner, 1994).

In CN-trapping assays performed on secondary alicyclic amines, such as the nefazodone *N*-dealkylation product, significant CN-adduct was found with an addition of 14 Da in the molecule (Argoti et al, 2005; Bauman et al, 2008). In our CN-trapping screening on *N*-dealkylated alicyclic compounds, significant CN-adducts with additional 14 Da were also observed and confirmed as the addition of a methylene group (data not reported). It has been suggested that this type of *N*-methylated CN-adduct from the secondary alicyclic amines was an experimental

DMD Fast Forward. Published on February 19, 2013 as DOI: 10.1124/dmd.112.050450

artifact or "metabonate" from *in vitro* microsomal incubation system (Gorrod and Sai, 1997; Li et al, 2006; Rousu and Tolonen, 2011; Barbara et al, 2012). In the case of *N*-methyl piperazines, there are two possible pathways for the formation of *N*-methyl piperazine CN-adducts (Figure 1). In pathway 1, the iminium ion is formed *via* α-carbon oxidation which could have potential toxicological implications (Sayre et al, 1997) and cause MBI of the P450 enzymes (Orr et al, 2012). In pathway 2, *N*-dealkylation results in the formation of secondary alicyclic amine which can react with formaldehyde and eventually lead to the formation of iminium ion. The CN-adduct from pathway 2 has been considered as the artifact from the *in vitro* system and irrelevant to *in vivo* (Gorrod and Sai, 1997; Rousu and Tolonen, 2011; Barbara et al, 2012). In the study reported here, we have evaluated the mechanism of CN-adduct formation in several piperazine containing compounds (Figure 2) with secondary and tertiary alicyclic amines. Piperazine compounds with [^{13}C]-labeled 4′-*N*-methyl group were used to quantify the contribution of each pathway to the formation of 4′-*N*-methyl piperazine CN-adduct in liver microsomal incubations. Furthermore, by identifying the one-carbon sources for the formation of 4′-*N*-methyl piperazine iminium ion, we have demonstrated the relevance of pathway 2 of CN-adduct formation to the *in vivo* system and thereby, to the potential ADR and MBI liabilities.

Materials and Methods

The 4′-*N*-alkyl piperazine compounds, tetrahydronapthalenes (**III**, **IV**), chromans (**VII** and **X-XIV)**, and the 4′-*N*-desmethyl piperazine compounds (**I**, **VI** and **IX**) were synthesized by AstraZeneca in Wilmington, DE. [^{13}C]Paraformaldehyde was purchased from Cambridge Isotope Laboratory (Andover, MA). HPLC water, methanol, potassium carbonate, and acetonitrile were purchased from Thermo Fisher Scientific Co. (Pittsburg, PA). Potassium

phosphate, dimethylsulfoxide (DMSO), LC/MS grade formic acid, ammonium formate, NADPH, magnesium chloride, sodium cyanoborohydride, triethylamine, bromoacetonitrile, potassium cyanide (KCN), potassium [^{13}C]carbonate, [^{13}C]methanol, and [^{13}C]formaldehyde and other chemical reagents used were purchased from Sigma-Aldrich (St. Louis, MO). Human liver microsomes were purchased from BD Gentest (San Jose, CA). Rat liver microsomes were purchased from CellzDirect (Austin, TX).

Synthesis of cyanide adduct standard (II) and 4′-*N*-[^{13}C]methyl piperazines (V and VIII).

Cyanomethyl piperazine analogue (**II**) was prepared by alkylation of the des-methyl precursor with bromoacetonitrile and potassium carbonate in DMSO. The [^{13}C] labeled adducts (**V** and **VIII**) were prepared by the reductive amination of the des-methyl precursor with [^{13}C]paraformaldehyde, sodium cyanoborohydride and triethylamine in methanol. The structures were confirmed by nuclear magnetic resonance (NMR), and the purity determined by LC/UV. The purity of the [^{13}C]-labeled compounds was greater than 98%.

Microsomal incubation

The CN-adduct formation was measured in human and rat liver microsomal (HLM and RLM, respectively) incubations. Unless specified, the 1-mL incubation media contained 10 μM of test compound, 1 mg/mL microsomal protein, 5 mM magnesium chloride, 5 mM KCN and 1 mM NADPH in 100 mM phosphate buffer, pH 7.4. Following pre-incubation at 37°C for 3 minutes, the reaction was initiated by the addition of the test compound. Equal volumes of cold acetonitrile were added to terminate the reaction at 30 minutes. Following the removal of

denatured protein by centrifugation, the supernatant was analyzed by liquid chromatography coupled with mass spectrometry (LC/MS).

To investigate the carbon source for *N*-methylated piperazine CN-adduct, a 10 μM of 4′-*N*-desmethyl piperazine compound (**I** or **IX**) was incubated with HLM in a phosphate buffer (pH 7.4) in the presence of KCN as described above, with either 5 mM of [^{13}C]-labeled potassium carbonate, 1% of methanol (v/v), or 1% of formaldehyde (v/v) included in the incubation. The reaction was initiated by the addition of NADPH. The control incubations that contained all components except KCN were performed. To determine the contribution of enzymes and NADPH to the formation of CN-adducts, compounds **I** or **IX** was also incubated in a solution containing all components except liver microsome or NADPH. In a separate study, compound **I** was incubated in HLM in the presence of 5 mM of [^{13}C]-labeled potassium carbonate, 5 mM of KCN with the addition of semicarbazide range from 0.3 to 3 mM to determine its impact on CN-adduct formation by removing aldehyde intermediate formed during the incubation.

LC/MS analysis

The CN-adducts formed in microsomal incubation were analyzed by ACQUITY Ultra Performance Liquid Chromatography (UPLC) system (Waters, Milford, MA) coupled with API 4000 QTRAP (Applied Biosystems, Foster City, CA) or LTQ Orbitrap mass spectrometer (Thermo Scientific, San Jose, CA). A 2.1×100 mm BEH C18 column with 1.7 μm particle size (Waters, Milford, MA) was used for the UPLC separation. Eluting solvents consisted of 0.1% formic acid and 5% acetonitrile in LC/MS grade water (A) and 0.1% formic acid in acetonitrile (B). The elution gradient, at flow rate of 0.2 mL/min, started with 0%B, linearly increased to 20%B in 4 minutes then linearly increased to 80%B in 3 minutes, to 95%B in another 2 minutes,

and held at 95% B for additional 2 minutes. The column was then equilibrated by washing with 100% A for 3 minutes.

API 4000 QTRAP analysis. The UPLC eluants were ionized under positive electrospray ionization (ESI) mode with curtain gas (CUR) set at 25, collision gas (CAD) at 10, ion spray voltage (IS) at 4500V, temperature (TEM) at 450ºC, ion source gas 1 (GS1) at 50, ion source gas 2 (GS2) at 50, declustering potential (DP) at 45V, enhanced potential (EP) at 10V, and collision cell exit potential (CXP) at 15V. Information dependent acquisition (IDA) was applied to trigger the enhanced product ionization (EPI) scan to obtain ms/ms fragmentation for ions exceeding 10000 counts per second (cps) from the Enhanced MS (EMS) scan or for ions exceeding 1000 cps from the neutral loss (NL) of 27 amu (NL-27) with a dwell time of 30 milliseconds. The collision energy (CE) for the NL and enhanced product ion (EPI) scans were set at 25 and 45V, respectively.

LTQ Orbitrap analysis. The CN-adduct structures were also analyzed by Orbitrap mass spectrometer under positive ESI mode with source voltage at 4kV, capillary temperature at 275 °C and the sheath gas flow rates at 60 arbitrary units. The Orbitrap Fourier transform mass spectrometer (FTMS) resolution was set at 15000 with a scan range at 50-600 *m/z*. Data dependent MS^2 and MS^3 fragmentation was obtained in the linear ion trap where the normalized CE was set at 35 with 0.23 activation Q and 30 millisecond activation time.

Data Processing

Accurate mass data acquisition, process and theoretical isotope spectra simulation were conducted with Xcalibur 2.1 (Thermo Scientific, San Jose, CA). Unit resolution mass data and NL-27 chromatograms were generated with Analyst version 1.4.2 (AB Sciex, Foster City, CA).

The natural abundance ratio of ^{13}C:^{12}C is 1.1:98.9. Theoretical ^{13}C relative abundance is determined by multiplying 1.1 by the number carbon atoms in the molecule. For example, for a molecule with 26 carbon atoms, the ^{13}C natural abundance in MS ion counts would be 28.6% of the ^{12}C ion counts. For the [^{13}C]-labeled compounds only a pure ^{13}C peak would be observed, and the changes in ^{13}C:^{12}C ratio of the CN-adduct with respect to the natural ^{13}C abundance of the reference cyanide adduct would indicate the extent of contribution from pathway 2 (Figure 1). When the contribution of pathway 1 is defined as α for the fraction of labeled ^{13}C remaining in the molecule and the contribution of pathway 2 as (1 – α) for the ^{12}C added to the molecule, the total ^{13}C in the molecule would be $\alpha + \beta\times(1 - \alpha)$, where β is the natural ^{13}C abundance gained from pathway 2. If A is defined as the total $^{13}C/^{12}C$ ratio, then $A = [\alpha + \beta\times(1 - \alpha)]/(1 - \alpha)$, from which, after rearranging the equation, the contribution of pathway 1 can be obtained, $\alpha = (A - \beta)/(1 + A - \beta)$, where A can be measured by mass spectrometer ion peak intensities and β derived from the natural ^{13}C abundance of ^{12}C in pathway 2.

Results

CN-adduct formation and structure confirmation.

Tetrahydronapthalene compounds. When 4′-*N*-desmethyl piperazine (**I**) was incubated in HLM or RLM with trapping agent KCN, a major CN-adduct peak at retention time (Rt) of 8.7 min was detected in LC/MS analysis monitoring NL-27 ions (Figure 3). This CN-adduct had a molecular ion at *m/z* 460.2716 ($C_{27}H_{34}O_2N_5$, Δ=2.0 ppm) which is consistent with the addition of a methyl and a CN-group. This CN-adduct peak matched the synthetic standard (**II)** peak in both Rt and MS characteristics (Figure 4). When 4′-*N*-methyl piperazine (**IV)** was incubated in HLM or RLM with KCN, three 4′-*N*-methyl piperazine CN-adduct peaks were detected in the NL-27

DMD Fast Forward. Published on February 19, 2013 as DOI: 10.1124/dmd.112.050450

ion chromatograms with the parent molecular ion at *m/z* 460 (Figure 5). Structural assignments of these three CN-adducts generated from **IV** were based on the ms/ms fragmentation patterns and the chromatographic peak retention time in comparison to the synthetic standard (**II)**. The m/z 433 fragment ion (m/z 460-HCN) from the molecular ion of CN-adduct and the benzoic-morpholine ions (*m/z* 190 or 188) were the signature fragments of these CN-adducts (Figure 6). When the CN-group was in the piperazine moiety, the intact benzoic-morpholine ion fragment (*m/z* 190) was observed (Figure 6A, C and D). The peak 1 generated a fragment at m/z 188 consistent with the benzoic-morpholine fragment following a neutral loss of HCN group from the morpholine ring (Figure 6B) therefore the CN-adduct group was assigned to morpholine. The Rt of peak 3 (Figure 5) and its fragmentation patterns (Figure 6D) matched with those of the synthetic standard **II** (Figure 4 and 6A, respectively) confirming that in peak 3 the CN-adduct was in the 4′-*N*-methyl group. The peak 2 generated a benzoic-morpholine fragment at *m/z* 190 (Figure 6C) but Rt did not match standard **II** indicating its CN-adduct is unlikely at the 4'-*N*-methyl group, therefore, the only other place left in piperazine to assign the CN-adduct would be at 2' or 3'-position.

When 4′-*N*-[^{13}C]methyl piperazine (**V**) was incubated with (rat or human) liver microsomes, the same peaks 1, 2 and 3 were also formed (Figure 7). Since the CN-adduct in the peak 1 was in the morpholine ring, the 4′-*N*-[^{13}C]methyl piperazine was intact in the molecule and there was no loss of [^{13}C]-label in the peak. In peak 2, [^{13}C]-methyl group was also retained demonstrating that the methyl piperazine CN-adducts in peak 2 was not preceded by 4′-*N*-demethylation, rather it was through α-oxidation at 2′ or 3′ position (pathway 1). However, in peak 3 significant amount of 4′-*N*-[^{13}C]methyl group was replaced by natural ^{12}C-methyl group (Figure 7),

indicating that the majority of methyl piperazine CN-adducts in peak 3 was formed after the 4′-*N*-demethylation (pathway 2) as illustrated in Figure 8.

Chroman compounds. As in the tetrahydronapthalene compounds under the same incubation conditions, 4′-*N*-desmethyl piperazine (**VI**) also generated a major 4′-*N*-methyl piperazine CN-adduct (Figure 9). Accurate mass analysis of this CN-adduct showed a molecular ion at *m/z* 480.2424 ($C_{26}H_{31}O_3N_5F$, Δ=2.7 ppm) consistent with the addition of methyl and CN-group to compound **VI**. Three major and one minor methyl piperazine CN-adduct peaks were observed in microsomal incubations of compound **VII** with KCN (Figure 10) and peak 3 (RT 8.8 min) matched the 4′-*N*-methyl piperazine CN-adduct peak from **VI** in Figure 9. The fragmentation pattern of the parent compound **VII** revealed that the fragment ion at *m/z* 277 was consistent with the chroman-8-(4′–*N*–methylpiperazine)-2-carbonyl moiety (Figure 11A) which could be used as signature fragment ion to locate the sites of CN-adducts. Fragmentation of 4′-*N*-methyl CN-adduct ion at *m/z* 480 from peaks 1, 2 and 3 (Figure 10) generated a product ion at *m/z* 453 as the result of neutral loss of 27 (HCN). Further fragmentation of the ion at *m/z* 453 generated a product ion at *m/z* 275 which is consistent with the chroman-8-(4′–*N*–methylpiperazine)-2-carbonyl moiety upon a neutral loss of HCN (Figures 11B, C and D), suggesting that the CN-adduct was in the piperazine moiety for peaks 1-3. Due to its low quantity, the minor methyl piperazine CN-adduct peak shown in Figure 10 did not trigger fragmentation and was not evaluated further. The ms/ms fragmentation pattern of the 4′-*N*-methyl piperazine CN-adduct (major peak in Figure 9) of *N*-desmethyl piperazine (**VI)** was similar to those of the 4′-*N*-methyl piperazine CN-adducts (peak 1- 3) generated from **VII** (data not shown). Similar results were observed for compounds **IX** and **X** (data not shown). When 4′-*N*-[^{13}C]methyl piperazine compound (**VIII**) was incubated in liver microsomes with KCN, significant [^{13}C]-methyl group

DMD Fast Forward. Published on February 19, 2013 as DOI: 10.1124/dmd.112.050450

was replaced by natural methyl group in CN-adduct peak 3, while in peaks 1 and 2 the 4′-*N*-[^{13}C]methyl group was retained in the CN-adducts (Figure 12), confirming that the CN-adduct in peak 3 was associated to 4′-*N* in the piperazine and that majority of CN-adduct in peak 3 was formed via pathway 2 as illustrated in Figure 13.

Contribution of pathway 2 in the formation of 4′-*N*-methyl piperazine CN-adduct

The contributions of pathways 1 and 2 to the formation of CN-adducts associated to 4′-*N*-methyl piperazine were estimated by measuring the ^{13}C/^{12}C ratio change following the incubation of [^{13}C]-methyl labeled compounds (**V** and **VIII**) with liver microsomes in the presence of KCN, and by analyzing the relationship between the extent of 4′-*N*-dealkylation and 4′-*N*-methyl piperazine CN-adduct formation. Following microsomal incubations of the 4′-*N*-[^{13}C]methyl piperazines (**V** or **VIII)** with KCN, a fraction of CN-adduct in peak 3 retained 4′-*N*-[^{13}C]methyl group suggesting bioactivation via pathway 1 (Figures 7 and 12). However, a significant proportion of 4′-*N*-[^{13}C]methyl group was replaced with natural 4′-*N*-[^{12}C]methyl group in the CN-adduct peak 3 indicating a significant contribution of pathway 2 (Figures 7 and 12). In HLM incubations, pathway 2 represented 75-80% of the 4′-*N*-methyl CN-adduct formation (Table 1). In RLM incubations with KCN, it represented 60-70%. The percent contribution by pathway 2 appeared to correlate with the extent of 4′-*N*-dealkylation of the piperazines. The peak areas of 4′-*N*-dealkylation products from compounds **X-XIV** was much smaller than those from compounds **III**, **IV**, **VII**, consistent with significantly lower levels of 4′-*N*-methyl piperazine CN-adduct formation from compounds **X-XIV** (Tables 2 and 3). After normalizing the peak areas of 4′-*N*-dealkylations products and 4′-*N*-methyl piperazine CN-adducts against parent peak areas in Tables 2 and 3 for HLM and RLM, respectively, the relationship between 4′-*N*-dealkylations and 4′-*N*-methyl piperazine CN-adduct formation was

DMD Fast Forward. Published on February 19, 2013 as DOI: 10.1124/dmd.112.050450

plotted in Figure 14 which clearly indicated that the extent of 4′-*N*-dealkylations were proportional to the level of 4′-*N*-methyl piperazine CN-adduct formations and that the tends were similar in HLM and RLM incubations. When these compounds were incubated in liver microsomes with KCN but in the absence of NADPH, no 4′-*N*-methyl piperazine CN-adducts were detected.

Incubation with [^{13}C]-labeled potential methyl donors

Two representative 4′-*N*-desmethyl piperazines **I** and **IX** were selected for the methyl donor experiment and to compare the extent of 4′-*N*-methyl piperazine CN-adduct formation. Compound **I** was from the tetrahydronapthalene series with its 4′-*N*-methyl piperazine (**IV)** showing extensive 4′-*N*-dealkylations in liver microsomal incubations. Compound **IX** was from the chroman series with its 4′-*N*-methyl piperazine (**X)** showing less extensive 4′-*N*-demethylation. Following the incubation of compound **I** or **IX** in HLM with KCN and [^{13}C]-labeled potential one-carbon donors, the relative amount [^{13}C]methyl group incorporated into the CN-adducts was evaluated by measuring the [^{13}C]-labeled 4′-*N*-methyl piperazines CN-adduct in the full scan accurate mass spectrum. The theoretical protonated molecular ion of 4′-*N*-methyl piperazine CN-adduct formed from **I** and **IX** should be at *m/z* 460 and 492 (Figures 15A and 16A), respectively. However, in HLM incubations with [^{13}C]-labeled potassium carbonate, methanol, or formaldehyde as the one-carbon donor, the majority of the 4′-*N*-methyl piperazine CN-adduct ions formed were 1 amu higher at *m/z* 461 and 493 (Figures 15B-D and Figures 16B-D, respectively), suggesting the incorporation of the ^{13}C isotope into the 4′-*N*-methylated CN-adducts. The extent of 4′-*N*-methyl piperazine CN-adduct formation was similar in both secondary amines (**I** and **IX)** but varied with the one-carbon donors (Figure 17). Formaldehyde and methanol appeared to be more effective as one-carbon donors than potassium carbonate.

DMD Fast Forward. Published on February 19, 2013 as DOI: 10.1124/dmd.112.050450

After 30-minute of HLM incubation in the presence of KCN and potassium carbonate as the one-carbon donor, only minor 4′-*N*-methyl piperazine CN-adduct peaks were formed. However, when formaldehyde or methanol was used significant levels of the parent compounds (**I** or **IX**) were converted to 4′-*N*-methyl piperazine CN-adduct. Under current CN-trapping conditions with excess of one-carbon donor in the microsomal incubation, formaldehyde and methanol generated similar amount of 4′-*N*-methyl piperazine CN-adduct as measured by peak area counts (Figure 17).

When **I** or **IX** was incubated in HLM with [^{13}C]-labeled methanol or potassium carbonate in the presence of KCN but in the absence of NADPH, no [^{13}C]-labeled 4′-*N*-methyl piperazine CN-adduct was detected, however, in the same HLM incubation in the absence of NADPH when [^{13}C]-labeled formaldehyde was used significant [^{13}C]-labeled 4′-*N*-methyl piperazine CN-adduct was formed (Figure 18). When incubated with the same [^{13}C]-labeled one-carbon donors in presence of NADPH and KCN but in the absence of HLM similar results were observed (Figure 19). When compound **I** was incubated in human liver microsomes in the presence of [^{13}C]-labeled potassium carbonate, KCN and the aldehyde trapping agent semicarbanzide, CN-adduction formation was significantly reduced (Figure 20).

Discussion

In this study, several approaches were applied to investigate the mechanisms involved in the formation of 4′-*N*-methyl piperazine CN-adducts. The first approach was the use of 4′-*N*-[^{13}C]methyl piperazine to determine the extent of pathway 2 involvement. Results from this study showed that a significant proportion of the 4′-*N*-[^{13}C]methyl groups in the piperazines were replaced by the natural [^{12}C]-methyl group in the CN-adducts when incubated with liver

DMD Fast Forward. Published on February 19, 2013 as DOI: 10.1124/dmd.112.050450

microsomes in the presence of KCN. The second approach involved the analysis of the relationship between the extent of 4′-*N*-dealkylation to the formation of 4′-*N*-methyl piperazine CN-adduct. This study demonstrated that in 4′-*N*-alkyl piperazines the level of 4′-*N*-methyl piperazine CN-adduct formation was proportional to the extent of 4′-*N*-dealkylation. In a separate study, different one carbon donors like [^{13}C]-labeled methanol, formaldehyde or potassium carbonate were evaluated to determine the carbon source for the 4′-*N*-methyl piperazine CN-adduct formation. The theoretical natural ^{13}C abundance in the piperazine CN-adduct standard (**II**) is 28% which matches the observed ^{13}C/^{12}C peak area ratio obtained in the mass spectrum (Figure 4 and Table 1). In 4′-*N*-[^{13}C]methyl piperazines (**V** and **VIII**), if the 4′-*N*-methyl piperazine CN-adduct was formed by direct reaction of the CN group with iminium ion following α-carbon oxidation (pathway 1), 100% of ^{13}C isotope would be retained in the 4′-*N*-methyl group. In case the CN-adduct was formed following 4′-*N*-dealkylation (pathway 2), the resulting 4′-*N*-methyl piperazine CN-adduct would not contain the synthetic [^{13}C]-carbon but the ^{12}C carbon plus natural abundance (~28%) of ^{13}C isotope in the molecule. Our results showed that the 4′-*N*-methyl piperazine CN-adducts (Peak 3 in Figures 7 and 12) from 4′-*N*-[^{13}C]methyl piperazines **V** and **VIII** contained high levels of ^{12}C carbon, indicating a significant contribution of pathway 2 to the 4′-*N*-methyl piperazine CN-adduct formation.

The relationship of piperazine 4′-*N*-dealkylation with 4′-*N*-methyl piperazine CN-adduct formation in the microsomal incubations was apparent when different 4′-*N*-substituted piperazines were compared. In microsomal incubations of the piperazine compounds containing a secondary 4′-nitrogen (**I**, **VI** and **IX**) in the presence of KCN, the 4′-*N*-methyl piperazine CN-adducts were the predominant CN-adducts. For 4′-*N*-alkyl piperazines (**III**, **IV**, **VII**, **X**-**XII** and **XIV**), the level of 4′-*N*-methyl piperazine CN-adduct formation appeared to be proportional to

the extent of 4′-*N*-dealkylation, suggesting that piperazine 4′-*N*-dealkylation was the rate limiting step in pathway 2. The trend of 4′-*N*-dealkylation and 4′-*N*-methyl piperazine CN-adduct formation in HLM and RLM appeared to be similar, however, the evaluation on 4′-*N*-dealkylation and 4′-*N*-methyl piperazine CN-adduct formation was only based on ion chromatogram peak area without synthetic standard references, the results presented are not fully quantitative.

To explore the potential carbon source for the formation of 4′-*N*-methyl piperazine CN-adducts, two 4′-*N*-desmethyl piperazine analogs (**I** or **IX**) were incubated in HLM with [^{13}C]-labeled potential one-carbon donors such as potassium carbonate, methanol, or formaldehyde. All three [^{13}C]-carbon sources resulted in the formation of 4′-*N*-[^{13}C]methyl piperazine CN-adducts from both **I** and **IX** in HLM incubations thereby confirming that solvents such as methanol and formaldehyde, or CO_2 dissolved in the incubation mixture could be the one-carbon source that reacted with 4′-*N*-dealkylated piperazines and formed corresponding 4′-*N*-methylenepiperazine iminium ions.

In Mannich reaction, the secondary amine reacts with aldehyde to generate reactive iminium ions which can be trapped by electron-rich alkenes (Tanaka et al. 2008; Abonia et al. 2013). Results from our study (Figures 18 and 19) demonstrate that formaldehyde reacting with secondary alicyclic amines such as **I** and **IX** can generate 4′-*N*-methyl piperazine CN-adducts in the absence of HLM or NADPH indicating this to be a direct Mannich reaction. Methanol can be an efficient one-carbon source as it has been shown to be readily oxidized to formaldehyde in microsomal incubations (Teschke et al. 1974). We have shown in this study that formation of 4′-*N*-methyl piperazine CN-adducts from the secondary alicyclic amines (**I**, **IX**) in the HLM incubation with methanol and KCN required NADPH, demonstrating that methanol oxidation to

formaldehyde was likely the first step of the one-carbon addition to those secondary alicyclic amines. Formaldehyde would appear to be more efficient one-carbon donor. However since the current CN-trapping study was qualitative with excess amount of one-carbon donors in the microsomal incubations, formaldehyde and methanol generated similar amount of 4′-*N*-methyl piperazine CN-adducts (Figure 17) and the kinetics of these reactions remain to be determined.

Compared to formaldehyde and methanol, CO_2 was less efficient as a one-carbon donor for the 4′-*N*-methyl piperazine CN-adduct formation (Figure 17). Primary and secondary amines have been reported to react with CO_2 to form carbamic acid in different *in vitro* and *in vivo* systems (Schaefer, 2006). However, the mechanism of CO_2 incorporation into alicyclic secondary amine to form the reactive iminium ion remains to be further investigated. Our preliminary ^{13}C NMR analysis indicated that formation of carbamic acid was not detectable when compound **I** was directly reacted with [^{13}C]-labeled potassium carbonate in aqueous solution (data not shown). Furthermore, our results demonstrated that this one-carbon addition to the alicyclic secondary amines (**I** and **IX**) was NADPH-dependent suggesting the involvement of P450 enzyme catalyzed bioactivation. We hypothesized that when using potassium carbonate as the one-carbon source in the liver microsomal incubation, the carbamic acid formation would be the first step of this methylation and this carbamic acid would need to be reduced to aldehyde then to alcohol which would then form methylene iminium ion following dehydration. If the aldehyde intermediate was eliminated by a trapping agent like semicarbazide it would likely reduce the iminium ion formation and thereby the *N*-methyl CN-adduct. Our preliminary results indicate that semicarbazide could decrease 4′-*N*-methyl piperazine CN-adducts formation in the HLM incubation of **I** with KCN and [^{13}C]-labeled potassium carbonate which further support the hypothesis of aldehyde formation by piperazine 4′-*N*-carbamic acid reduction.

Iminium ions from piperazine α-carbon oxidation (pathway 1) have been considered as a bioactivation process while those from pathway 2 as experimental artifact due to the potential interaction with formaldehyde in the incubation buffer (Gorrod and Sai, 1997; Li et al, 2006; Rousu and Tolonen, 2011; Barbara et al, 2012). However, the biological and toxicological implications of iminium ions *via* pathway 2 require further investigation for the following reasons. First, in the case of Methanol and carbon dioxide, P450 enzymes are likely involved in the one-carbon addition to the alicyclic secondary amines resulting in piperazine *N*-methylene iminium ion formation. Second, the potential one-carbon donors can be found *in vivo* since carbon dioxide is abundant as carbonate anion in the body. Methanol occurs naturally in human body as a product of metabolism and through intake of fruits, vegetables, and alcoholic beverages (Shelby et al, 2004; Turner et al, 2006). Methanol levels in human blood range from 0.25-4.7 mg/L or 8-145 μM (Cook et al, 1991; Batterman and Franzblau, 1997). The endogenous concentration of formaldehyde in the blood of rat, monkey and human is about 100 μM, and the level in rat liver is 2-4 folds higher (Heck and Casanova, 2004). The formaldehyde and methanol concentrations used in our study were 60 and 300 μM, respectively. Furthermore, the one-carbon addition products have been found in rat blood and urine dosed with homopiperazine (Martin et al, 2012). These naturally abundant one-carbon sources could potentially fuel the bioactivation of secondary amines to form *N*-methylene iminium ions *in vivo*. The resulting reactive *N*-methylene iminium ions could potentially bind to macromolecules which is a concern because of potential liability for mechanism based inactivation and/or idiosyncratic toxicity. Therefore, pathway 2 is relevant to *in vivo* bioactivation and warrant further investigations on its association to adverse drug reactions.

Acknowledgements

We would like to thank Doug Burdette, Richard Thompson, Emre Isin, Ulf Bredberg, and Neal Castagnoli, and Scott Grimm, AstraZeneca and Ned Heindel, Lehigh University for comments on the manuscript; M. Edward Pierson and Peter R. Bernstein, AstraZeneca for providing the test compounds.

Authorship Contributions

Participated in research design: Zhang, Resuello, Guo, Powell, Elmore and Hu

Conducted experiments: Zhang, Resuello, Guo, Powell, Elmore and Hu

Performed data analysis: Zhang, Resuello, Guo, Powell, Elmore and Hu

Wrote or contributed to the writing of the manuscript: Zhang, Resuello, Guo, Powell, Elmore, Hu and Vishwanathan

References

Abonia R, Castillo J, Insuasty B, Quiroga J, Nogueras M, and Cobo J. (2013) Efficient catalyst-free four-component synthesis of novel γ-aminoethers mediated by a mannich type reaction. *ACS Comb Sci* **15**:2-9.

Argoti D, Liang L, Conteh A, Chen L, Bershas D, Yu CP, Vouros P, and Yang E. (2005) Cyanide trapping of iminium ion reactive intermediates followed by detection and structure identification using liquid chromatography-tandem mass spectrometry (LC-MS/MS). *Chem Res Toxicol* **18**:1537-1544.

Barbara JE, Kazmi F, Muranjan S, Toren PC, and Parkinson A. (2012) High Resolution Mass Spectrometry Elucidates Metabonate (False Metabolite) Formation from Alkylamine Drugs during In Vitro Metabolite Profiling. *Drug Metab Dispos* **40**:1966-1975.

Batterman SA and Franzblau A. (1997) Time-resolved cutaneous absorption and permeation rates of methanol in human volunteers. *Int Arch Occup Environ Health* **70**:341-351.

Bauman JN, Frederick KS, Sawant A, Walsky RL, Cox LM, Obach RS, and Kalgutkar AS. (2008) Comparison of the bioactivation potential of the antidepressant and hepatotoxin nefazodone with aripiprazole, a structural analog and marketed drug. *Drug Metab Dispos* **36**:1016-1029.

Colowick SP, Kaplan NO, and Ciotti MM. (1951) The reaction of pyridine nucleotide with cyanide and its analytical use. *J Biol Chem* **191**:447-459.

Cook MR, Bergman FJ, Cohen HD, Gerkovich MM, Graham C, Harris RK, and Siemann LG. (1991) Effects of methanol vapor on human neurobehavioral measures. *Res Rep Health Eff Inst* **(42)**:1-45.

Evans DC, Watt AP, Nicoll-Griffith DA, and Baillie TA. (2004) Drug-protein adducts: an industry perspective on minimizing the potential for drug bioactivation in drug discovery and development. *Chem Res Toxicol* **17**:3-16.

Gorrod JW and Sai Y. (1997) Recognition of novel artifacts produced during the microsomal incubation of secondary alicyclic amines in the presence of cyanide. *Xenobiotica* **27**:389-399.

Gorrod JW and Aislaitner G. (1994) The metabolism of alicyclic amines to reactive iminium ion intermediates. *Eur J Drug Metab Pharmacokinet* **19**:209-217.

Heck H and Casanova M. (2004) The implausibility of leukemia induction by formaldehyde: a critical review of the biological evidence on distant-site toxicity. *Regul Toxicol Pharmacol* **40**:92-106.

Kalgutkar AS and Soglia JR. (2005) Minimising the potential for metabolic activation in drug discovery. *Expert Opin Drug Metab Toxicol* **1**:91-142.

Kaplowitz N. (2005) Idiosyncratic drug hepatotoxicity. *Nat Rev Drug Discov* **4**:489-499.

Kumar S, Kassahun K, Tschirret-Guth RA, Mitra K, and Baillie TA. (2008) Minimizing metabolic activation during pharmaceutical lead optimization: progress, knowledge gaps and future directions. *Curr Opin Drug Discov Devel* **11**:43-52.

Li C, Surapaneni S, Zeng Q, Marquez B, Chow D, and Kumar G. (2006) Identification of a novel in vitro metabonate from liver microsomal incubations. *Drug Metab Dispos* **34**:901-905.

Martin S, Lenz EM, Temesi D, Wild M, and Clench MR. (2012) Reaction of homopiperazine with endogenous formaldehyde: a carbon hydrogen addition metabolite/product identified in rat urine and blood. *Drug Metab Dispos* **40**:1478-1486.

Murphy PJ. (1973) Enzymatic oxidation of nicotine to nicotine 1'(5') iminium ion. A newly discovered intermediate in the metabolism of nicotine. *J Biol Chem* **248**:2796-2800.

Orr ST, Ripp SL, Ballard TE, Henderson JL, Scott DO, Obach RS, Sun H, and Kalgutkar AS. (2012) Mechanism-based inactivation (MBI) of cytochrome P450 enzymes: structure-activity relationships and discovery strategies to mitigate drug-drug interaction risks. *J Med Chem* **55**:4896-4933.

Rousu T and Tolonen A. (2011) Characterization of cyanide-trapped methylated metabonates formed during reactive drug metabolite screening in vitro. *Rapid Commun Mass Spectrom* **25**:1382-1390.

Sayre LM, Engelhart DA, Nadkarni DV, Manoj Babu MK, Flammang AM, and McCoy GD. (1997) The role of iminium-enamine species in the toxication and detoxication of cyclic tertiary amines. *NIDA Res Monogr* **173**:106-127.

Schaefer WH. (2006) Reaction of primary and secondary amines to form carbamic acid glucuronides. *Curr Drug Metab* **7**:873-881.

Shelby M, Portier C, Goldman L, Moore J, Iannucci A, Jahnke G, Donkin S, and NTP-CERHR Expert Panel. (2004) NTP-CERHR expert panel report on the reproductive and developmental toxicity of methanol. *Reprod Toxicol* **18**:303-390.

Smith DA and Obach RS. (2009) Metabolites in safety testing (MIST): considerations of mechanisms of toxicity with dose, abundance, and duration of treatment. *Chem Res Toxicol* **22**:267-279.

Tanaka Y, Hasui T, and Suginome, M. (2008) Diarylborinic acid derivatives as a catalytic iminium ion generator in the mannich-type reaction using secondary amines, aldehydes, and ketene silyl acetals. *Synlett* **8**:1239-1242

Turner C, Spanel P, and Smith D. (2006) A longitudinal study of methanol in the exhaled breath of 30 healthy volunteers using selected ion flow tube mass spectrometry, SIFT-MS. *Physiol Meas* **27**:637-648.

Teschke R, Hasumura Y, Lieber CS. (1974) NADPH-dependent oxidation of methanol, ethanol, propanol and butanol by hepatic microsomes. *Biochem Biophys Res Commun* **23**:851-7.

Ulrich RG. (2007) Idiosyncratic toxicity: a convergence of risk factors. *Annu Rev Med* **58**:17-34.

Walgren JL, Mitchell MD, and Thompson DC. (2005) Role of metabolism in drug-induced idiosyncratic hepatotoxicity. *Crit Rev Toxicol* **35**:325-361.

Waring JF and Anderson MG. (2005) Idiosyncratic toxicity: mechanistic insights gained from analysis of prior compounds. *Curr Opin Drug Discov Devel* **8**:59-65.

Legends for Figures

Figure 1. Proposed mechanism of 4′-*N*-methyl piperazine CN-adduct formation in liver microsomal incubations

Figure 2. Structures of piperazine compounds studied

Figure 3. NL-27 ion chromatogram monitoring *m/z* 446 ion (4′-*N*-desmethyl piperazine CN-adduct, early small peak) and *m/z* 460 ion (4′-*N*-methyl piperazine CN-adduct, major peak) in HLM (A) and RLM (B) incubations of compound **I** in the presence of KCN

Figure 4. NL-27 ion chromatogram monitoring *m/z* 460 (blue for ^{12}C) and 461 (red for ^{13}C) ions of the synthetic standard (**II**)

Figure 5. NL-27 ion chromatogram monitoring *m/z* 460 ions (4′-*N*-methyl piperazine CN-adducts) in HLM (A) and RLM (B) incubations of compound **IV** in the presence of KCN

Figure 6. MS^2 fragmentation patterns of 4′-*N*-methyl piperazine CN-adducts of compound (**IV**). A, synthetic standard (2); B-D, CN adduct peaks 1-3, respectively (presented in Figure 5)

Figure 7. NL-27 ion chromatogram monitoring *m/z* 460 (blue for ^{12}C) and *m/z* 461 (red for ^{13}C) ions of 4′-*N*-methyl piperazine CN-adducts in HLM (A) and RLM (B) incubations of compound **V** in the presence of KCN

Figure 8. Proposed pathway of tetrahydronapthalene compound (**V**) 4′-*N*-methyl piperazine CN-adduct formation in liver microsomal incubations in the presence of KCN

Figure 9. NL-27 ion chromatogram monitoring *m/z* 466 ion (4′-*N*-desmethyl piperazine CN-adduct, early small peak) and *m/z* 480 ion (4′-*N*-methyl piperazine CN-adduct, major peak) in HLM (A) and RLM (B) incubations of compound **VI** in the presence of KCN

Figure 10. NL-27 ion chromatogram monitoring *m/z* 480 ions (4′-*N*-methyl piperazine CN-adducts) in HLM (A) and RLM (B) incubations of compound **VII** in the presence of KCN

Figure 11. Fragmentation patterns. (A) MS^2 fragmentation pattern of parent (**VII)** molecular ion (m/z 455); (B-D) MS^3 fragmentation pattern of **VII** CN-adducts: fragmentation of *m/z* 453 (resulted from the neutral loss of HCN from the molecular ion of *m/z* 480 in peaks 1-3, respectively; Peaks 1-3 refers to the peaks in Figure 10)

Figure 12. NL-27 ion chromatogram monitoring m/z 480 (blue for ^{12}C) and *m/z* 481 (red for ^{13}C) ions of 4′-*N*-methyl piperazine CN-adducts in HLM (A) and RLM (B) incubations of compound **VIII** in the presence of KCN

Figure 13. Proposed pathway of chroman compound (**VIII**) 4′-*N*-methyl piperazine CN-adduct formation in liver microsomal incubations in the presence of KCN

Figure 14. Relationship of piperazine 4′-*N*-dealkylation to 4′-*N*-methyl piperazine adduct formation. Each data point represented one compound in HLM or RLM incubations

Figure 15. Formation of 4′-*N*-[^{13}C]methyl piperazine CN-adduct in the HLM incubations of compound **I** in the presence of KCN with different [^{13}C]-labeled one-carbon donors. (A) Simulated isotope spectrum for molecular ion of natural 4′-*N*-methyl piperazine CN-adduct; (B-D) Isotope spectra for molecular ion of 4′-*N*-methyl piperazine CN-adduct in HLM incubations

DMD Fast Forward. Published on February 19, 2013 as DOI: 10.1124/dmd.112.050450

with KCN in the presence of 5 mM of [^{13}C]-labeled potassium carbonate, 1% (v/v) of [^{13}C]-methanol or 1% (v/v) of formaldehyde, respectively.

Figure 16 Formation of 4′-*N*-[^{13}C]methyl piperazine CN-adduct in the HLM incubation of compound **IX** in the presence of KCN with [^{13}C]-labeled one-carbon donors. (A) Simulated isotope spectrum for molecular ion of 4′-*N*-methyl piperazine CN-adduct; (B-D) Isotope spectra for molecular ion of 4′-*N*-methyl piperazine CN-adduct in HLM incubations with KCN in the presence of 5 mM of [^{13}C]-labeled potassium carbonate, 1% (v/v) of [^{13}C]-methanol or 1% (v/v) of formaldehyde, respectively.

Figure 17 Selected ion chromatogram on the extent of 4′-*N*-[^{13}C]methyl piperazine CN-adduct formation from compound **I** (left column) and **IX** (right column), respectively, in HLM incubations with KCN, and including 5 mM of [^{13}C]-labeled potassium carbonate (top row), 1% (v/v) of [^{13}C]-methanol (middle row) or 1% (v/v) of [^{13}C]-formaldehyde (bottom row), respectively. Peak I, compound **I** at *m/z* 421.2607; Peak I-MCN, 4′-*N*-[^{13}C]methyl piperazine CN-adduct of **I** at *m/z* 461.2733; Peak IX, compound **IX** at *m/z* 453.2491; Peak IX-MCN, 4′-*N*-[^{13}C]methyl piperazine CN-adduct of **IX** at *m/z* 493.2629; AA, integrated peak area (count per second).

Figure 18 Selected ion chromatogram on the extent of 4′-*N*-[^{13}C]methyl piperazine CN-adduct formation from compound **I** (left column) and **IX** (right column), respectively, in incubations without HLM, in the presence of NADPH and KCN, and including 5 mM of [^{13}C]-labeled potassium carbonate (top row), 1% (v/v) of [^{13}C]-methanol (middle row) or 1% (v/v) of [^{13}C]-formaldehyde (bottom row), respectively. Peak I, compound **I** at *m/z* 421.2607; Peak I-MCN, 4′-*N*-[^{13}C]methyl piperazine CN-adduct of **I** at *m/z* 461.2733; Peak IX, compound **IX** at *m/z*

453.2491; Peak IX-MCN, 4′-*N*-[^{13}C]methyl piperazine CN-adduct of **IX** at *m/z* 493.2629. Peak ×, interference peak.

Figure 19 Selected ion chromatogram on the extent of 4′-*N*-[^{13}C]methyl piperazine CN-adduct formation from compound **I** (left column) and **IX** (right column), respectively, in HLM incubations without NADPH, in the presence of KCN and including 5 mM of [^{13}C]-labeled potassium carbonate (top row), 1% (v/v) of [^{13}C]-methanol (middle row) or 1% (v/v) of [^{13}C]-formaldehyde (bottom row), respectively. Peak I, compound **I** at *m/z* 421.2607; Peak I-MCN, 4′-*N*-[^{13}C]methyl piperazine CN-adduct of **I** at *m/z* 461.2733; Peak IX, compound **IX** at *m/z* 453.2491; Peak IX-MCN, 4′-*N*-[^{13}C]methyl piperazine CN-adduct of **IX** at *m/z* 493.262.

Figure 20 Inhibitory effect of semicarbazide on 4′-*N*-[^{13}C]methyl piperazine CN-adduct formation in the HLM incubation of compound **I** with KCN in the presence of 5 mM [^{13}C]-labeled potassium carbonate.

DMD Fast Forward. Published on February 19, 2013 as DOI: 10.1124/dmd.112.050450

Table 1. Relative levels of ^{12}C and ^{13}C in 4′-*N*-methyl piperazine CN adducts from [^{13}C]-labeled compounds (**V**) and (**VIII**) in microsomal incubations with the presence of KCN.

Parent Compound	Microsome	$^{13}C/^{12}C$ ratio of CN-adducts (A)	Pathway 1 Contribution (α)	Pathway 2 (artifact) Contribution (1-α)
II (standard)	none	0.28	--	--
V	HLM	0.62	0.24	0.76
V	RLM	0.94	0.39	0.61
VIII	HLM	0.49	0.17	0.83
VIII	RLM	0.72	0.30	0.70

DMD Fast Forward. Published on February 19, 2013 as DOI: 10.1124/dmd.112.050450

Table 2. Relationship of 4′-*N*-methyl piperazine CN-adduct formation in HLM to the extent of 4′-*N*-dealkyation in piperazine compounds

Compound	Parent		Piperazine 4′-*N*-dealkylated Products[1]		4′-*N*-methyl piperazine CN-adducts	
	m/z	Peak Area[2]	*m/z*	Peak Area[2]	*m/z*	Peak Area[2]
III	449	690	421	25	460	58
IV	435	648	421	109	460	250
VII	455	471	441	18	480	52
X	467	62	453	0.6	492	0.1
XI	481	63	453	0.8	492	0.1
XII	495	107	453	0.7	492	0.1
XIII	495	60	453	0.3	492	1.0
XIV	509	79	453	0.4	492	0.1

[1]The dealkylation products were from HLM incubations without KCN. [2]Peak area was expressed as ion count per second (cps) × 10^6.

DMD Fast Forward. Published on February 19, 2013 as DOI: 10.1124/dmd.112.050450

Table 3. Relationship of 4′-*N*-methyl piperazine CN-adduct formation in RLM to the extent of 4′-*N*-dealkyation in piperazine compounds

Compound	Parent		Piperazine 4′-*N*-dealkylated Products[1]		4′-*N*-methyl piperazine CN-adducts	
	m/z	Peak Area[2]	*m/z*	Peak Area[2]	*m/z*	Peak Area[2]
III	449	674	421	96	460	36
IV	435	722	421	247	460	273
VII	455	522	441	58	480	54
X	467	81	453	0.8	492	0.3
XI	481	99	453	1.4	492	0.3
XII	495	124	453	0.8	492	0.1
XIII	495	61	453	0.8	492	0.5
XIV	509	89	453	1.6	492	0.5

[1]The dealkylation products were from RLM incubations without KCN. [2]Peak area was expressed as ion count per second (cps) × 10^6.

Figure 1

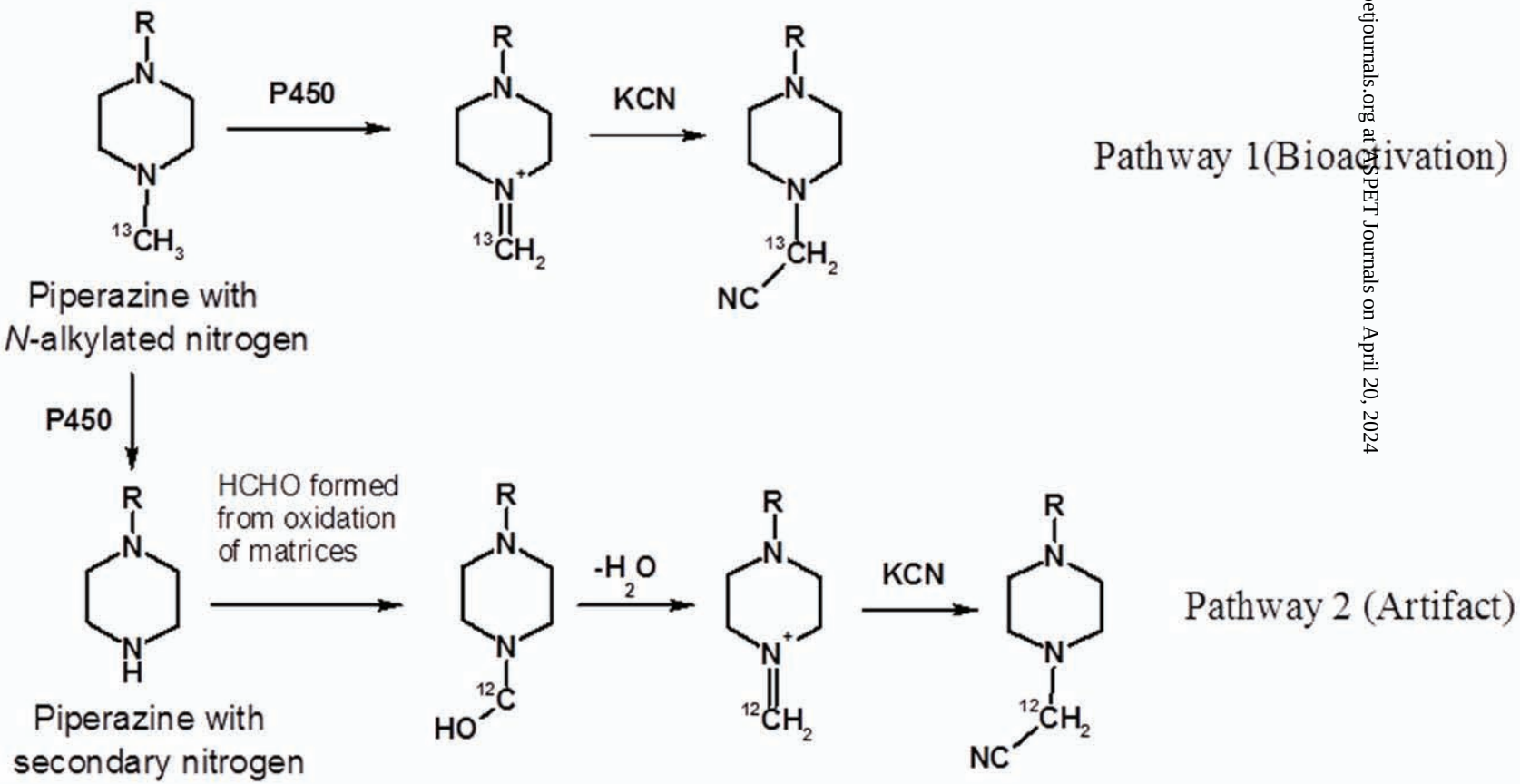

Figure 2

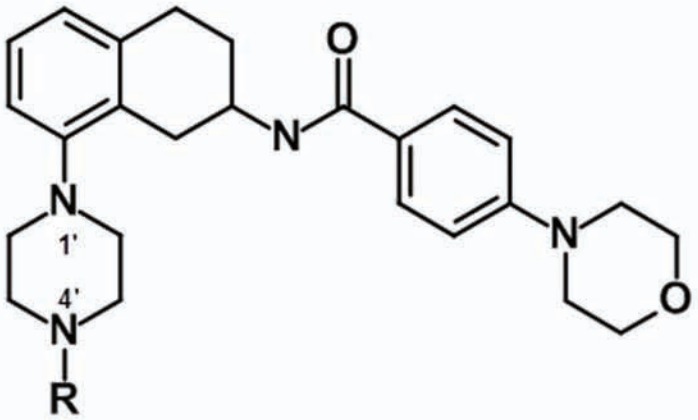

Tetrahydronapthalene	R
I	H
II	CH_2CN
III	CH_2CH_3
IV	CH_3
V	$^{13}CH_3$

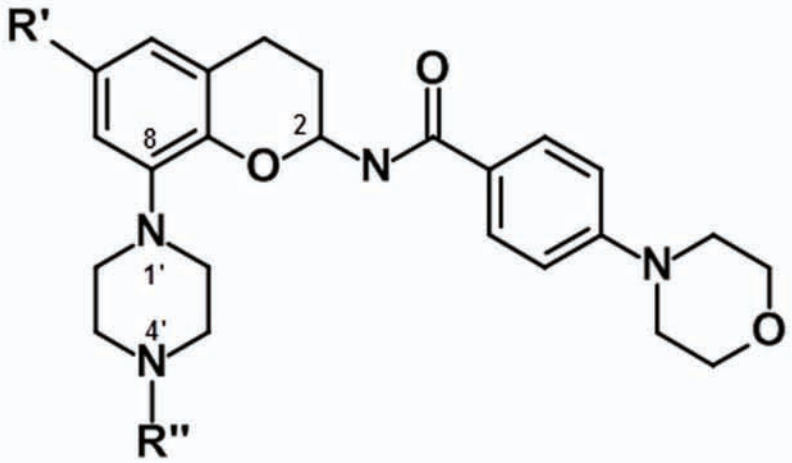

Chroman	R′	R″
VI	F	H
VII	F	CH_3
VIII	F	$^{13}CH_3$
IX	CH_3O	H
X	CH_3O	CH_3
XI	CH_3O	CH_2CH_3
XII	CH_3O	$CH(CH_3)_2$
XIII	CH_3O	$(CH_2)_2CH_3$
XIV	CH_3O	$(CH_2)_3CH_3$

Figure 3

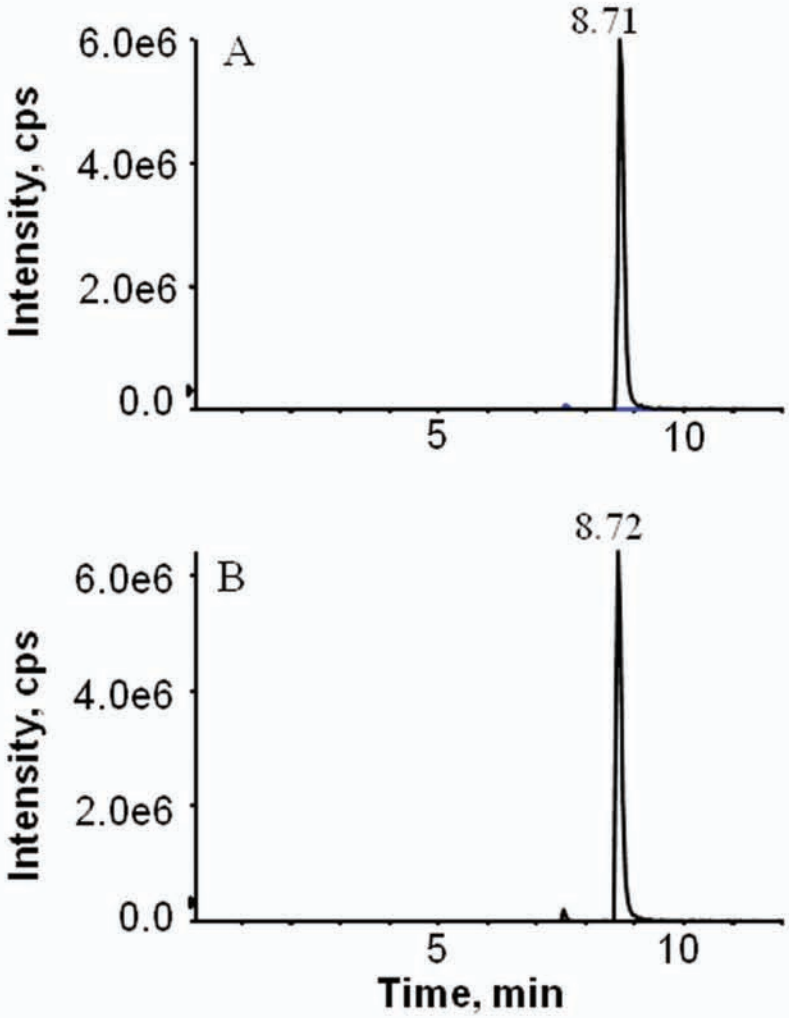

Figure 4

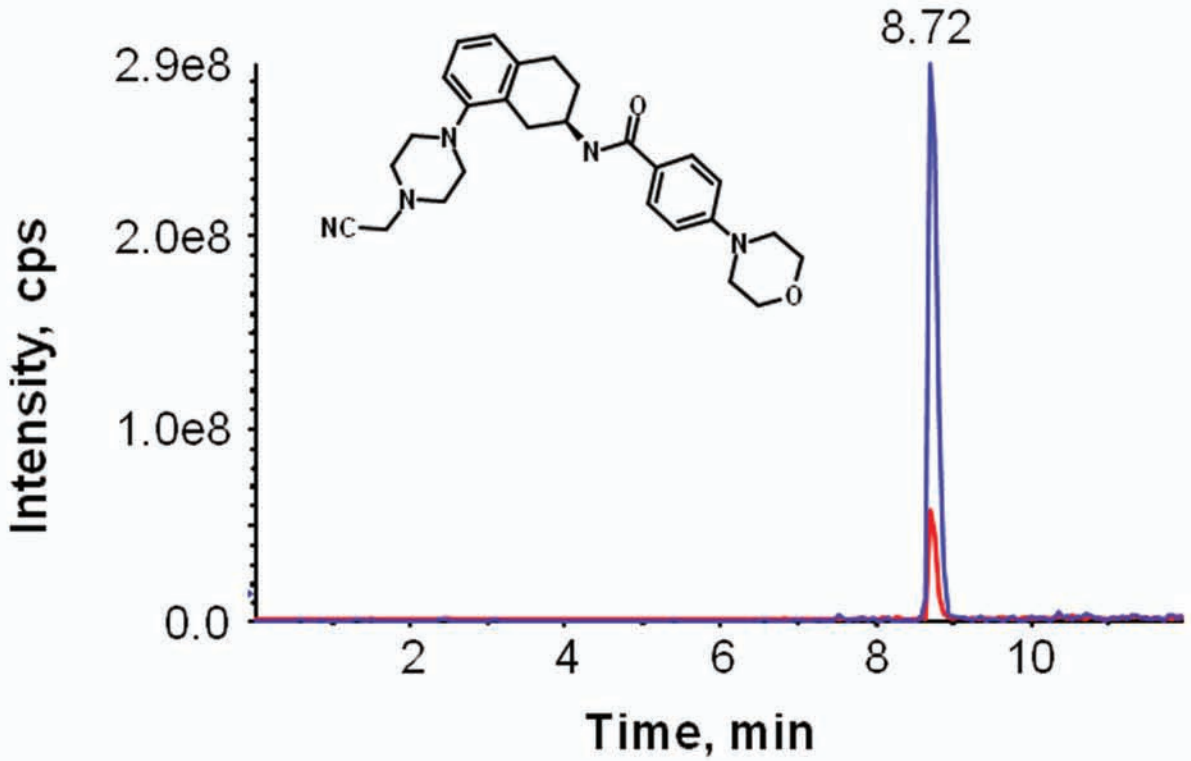

Figure 5

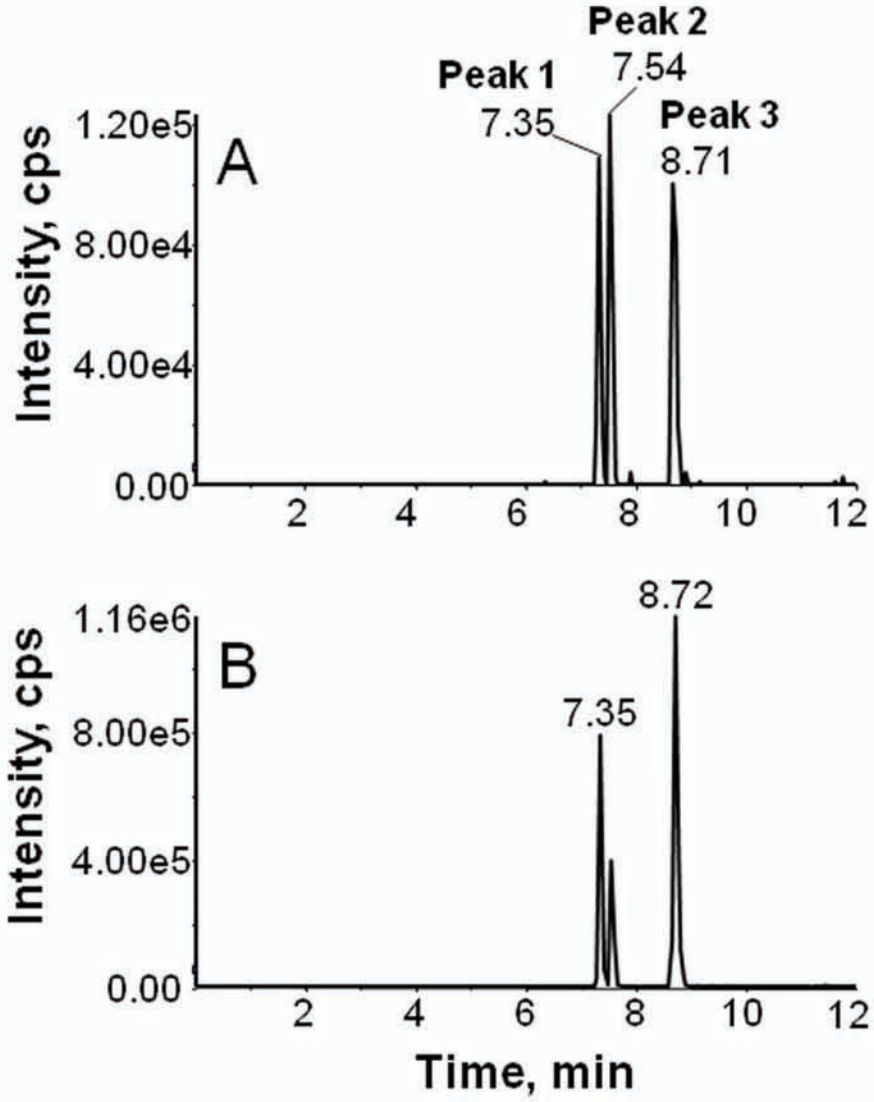

Figure 6

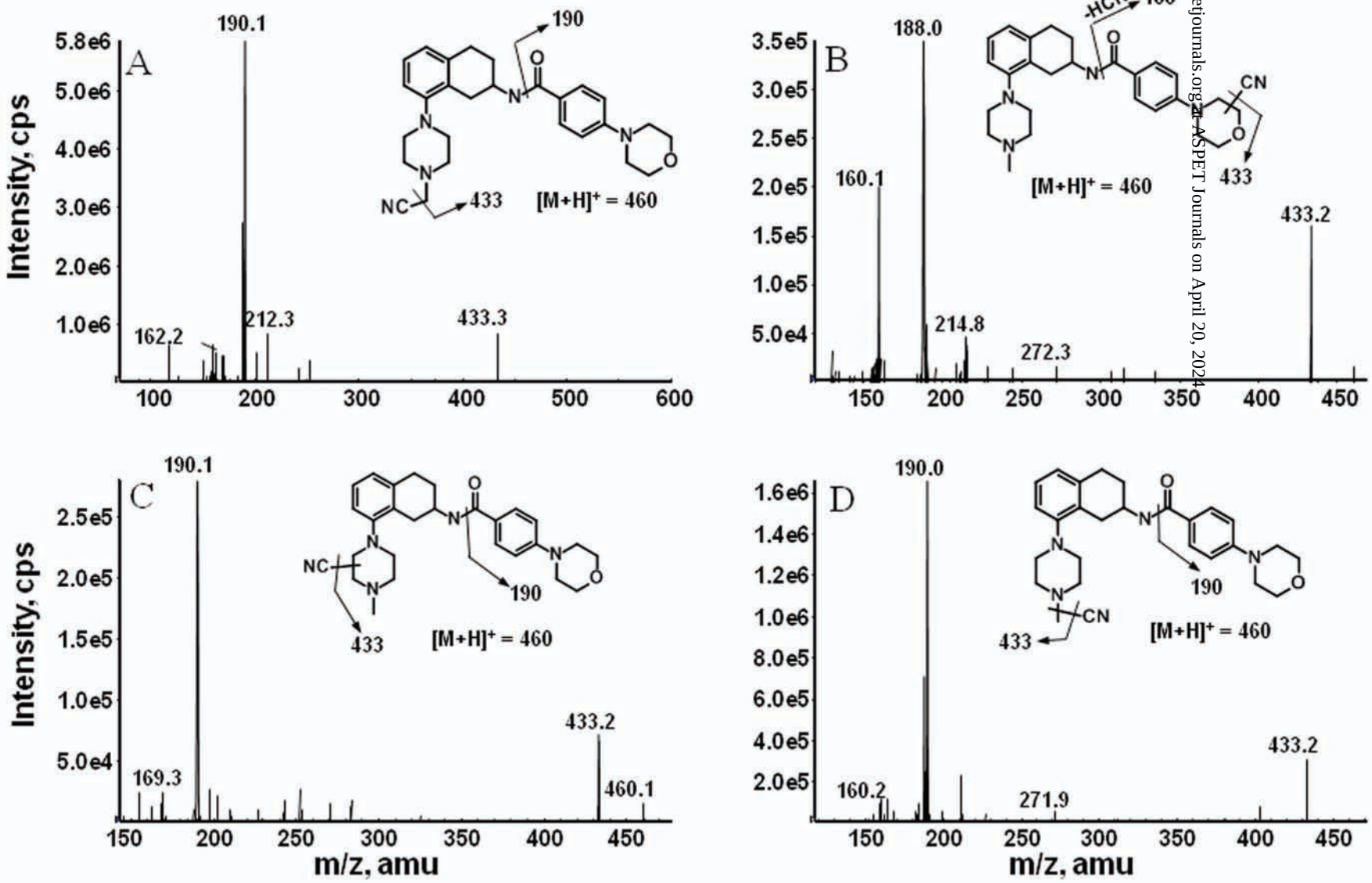

Figure 7

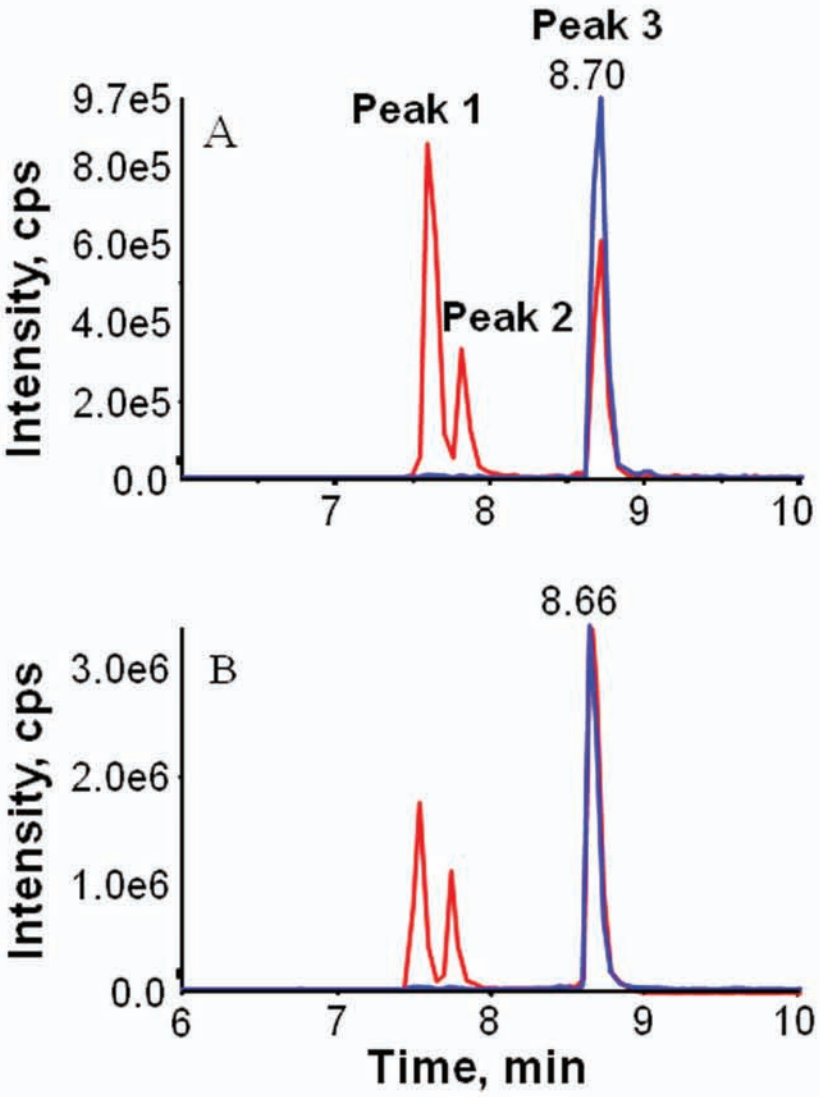

Figure 8

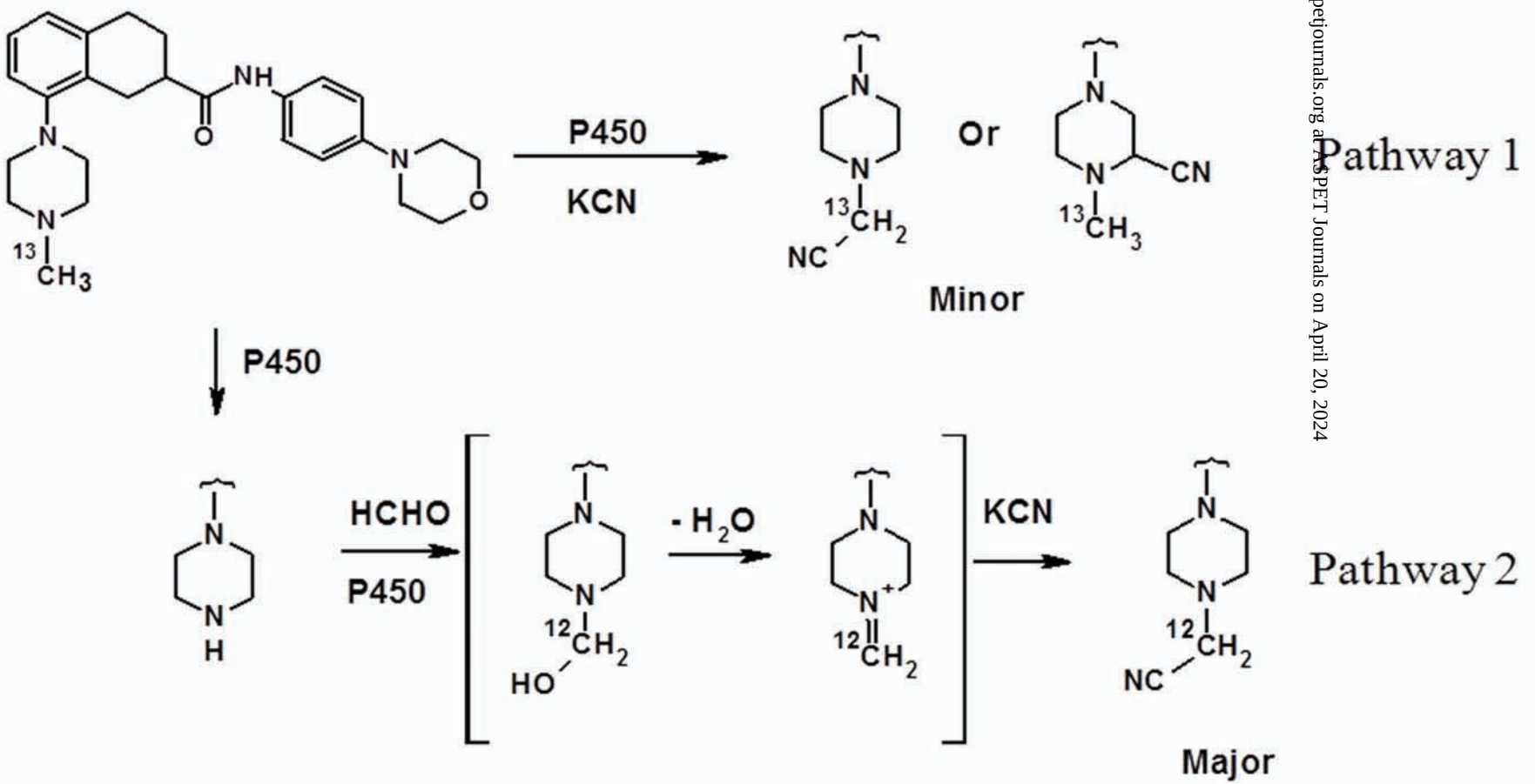

Figure 9

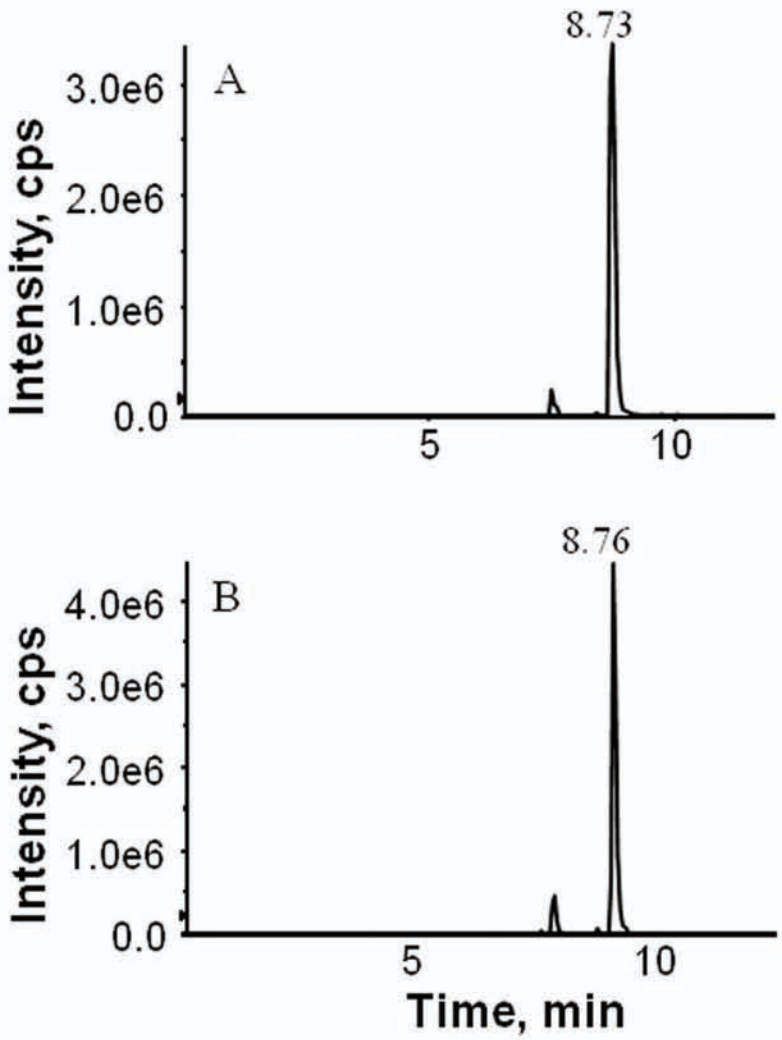

Figure 10

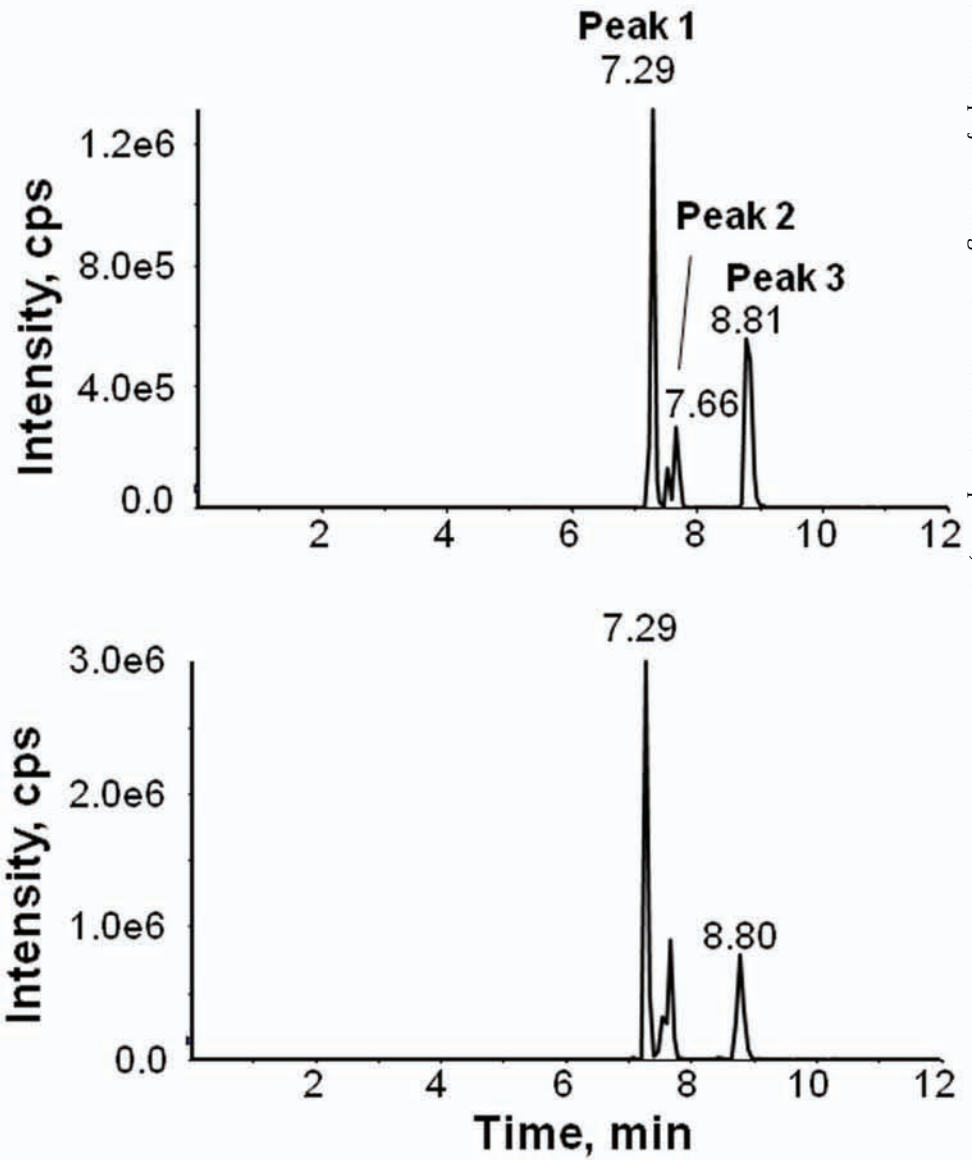

Figure 11

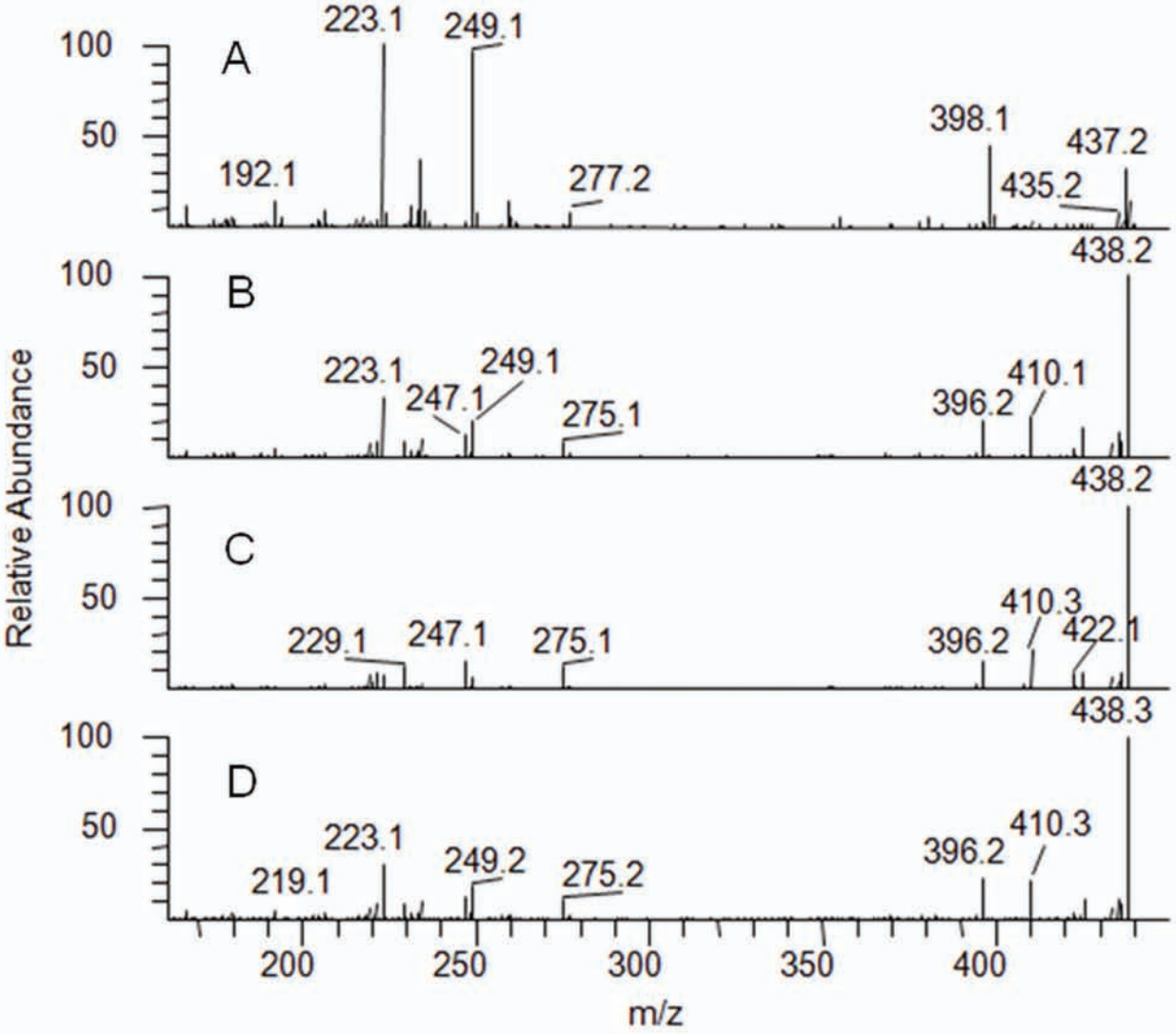

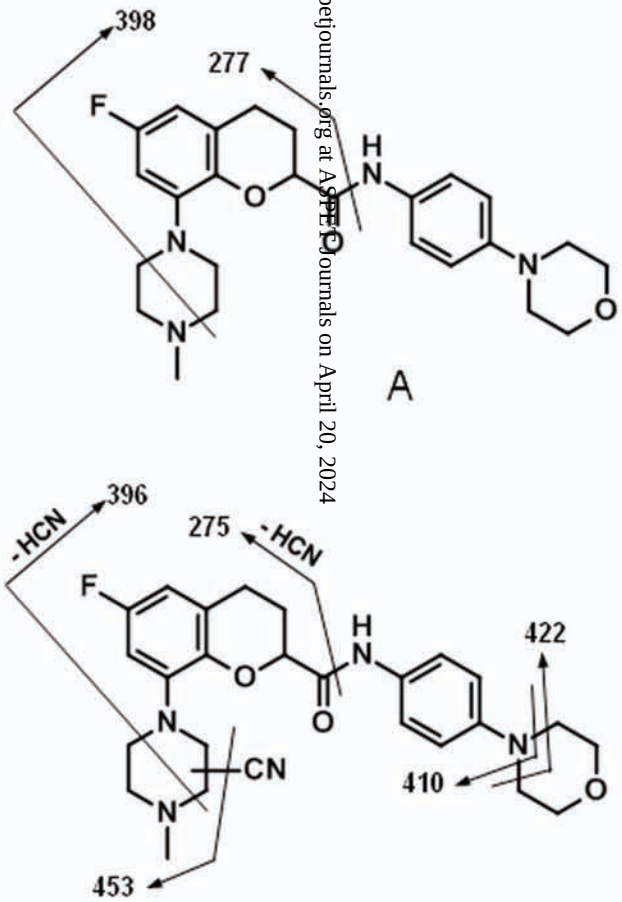

Figure 12

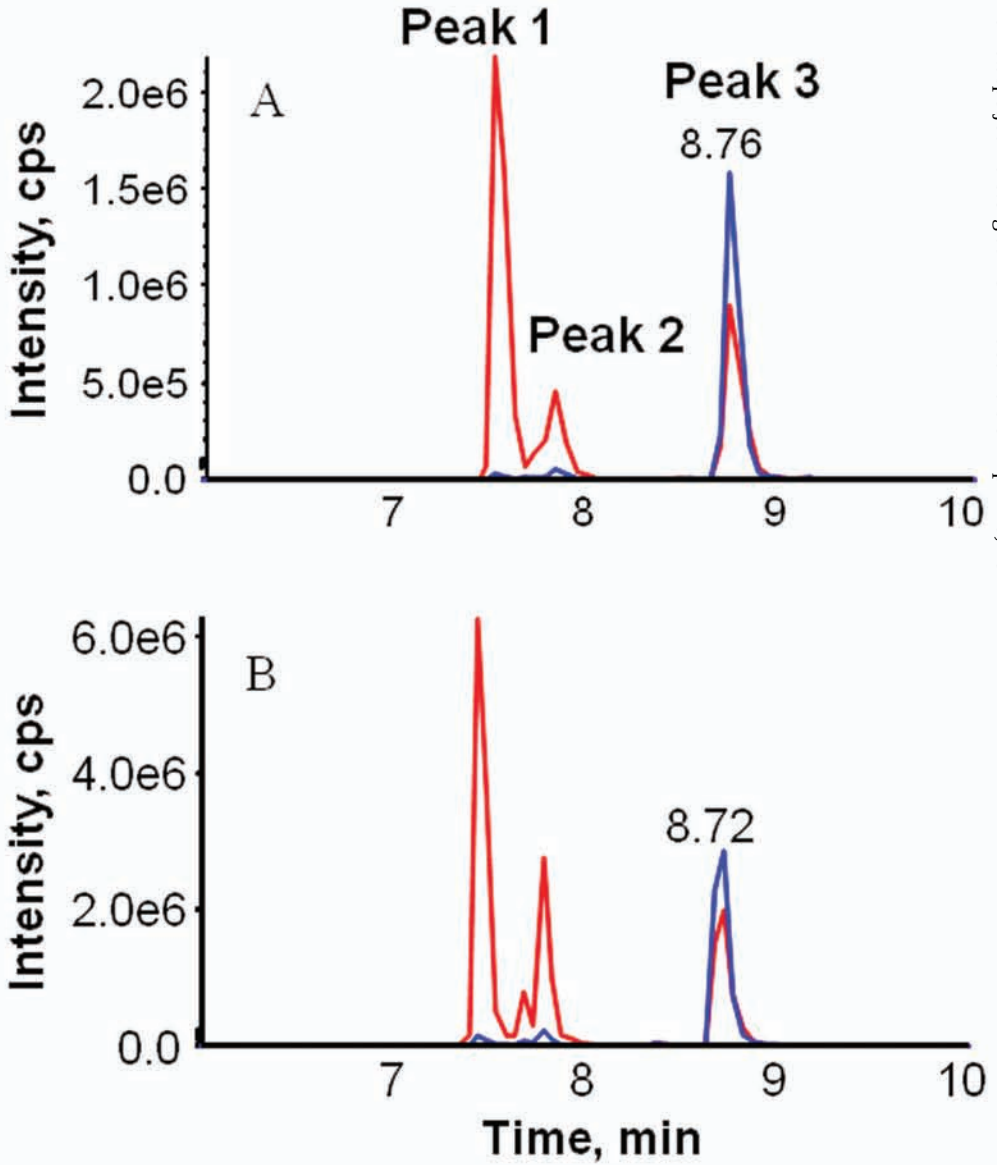

Figure 13

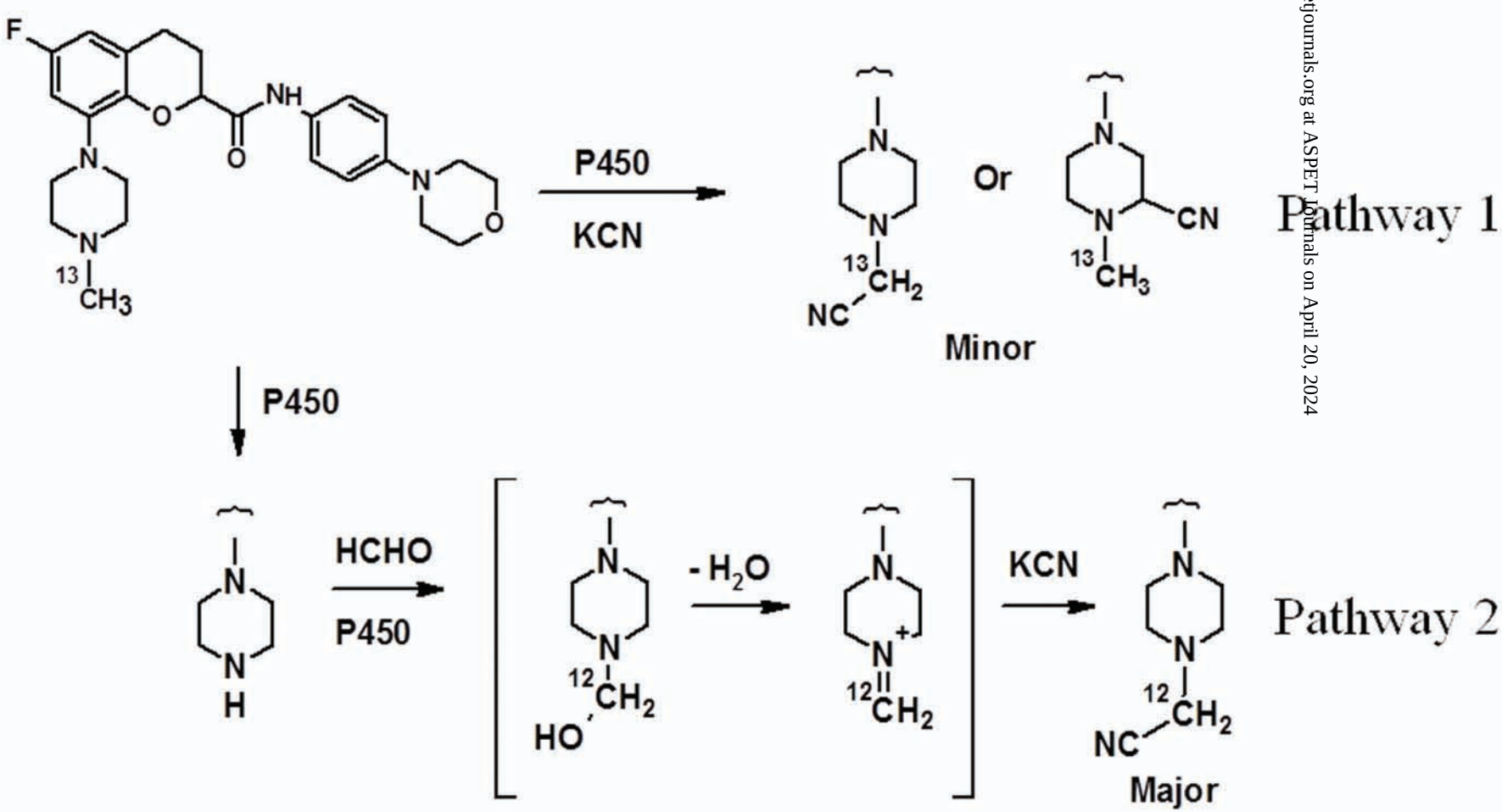

Figure 14

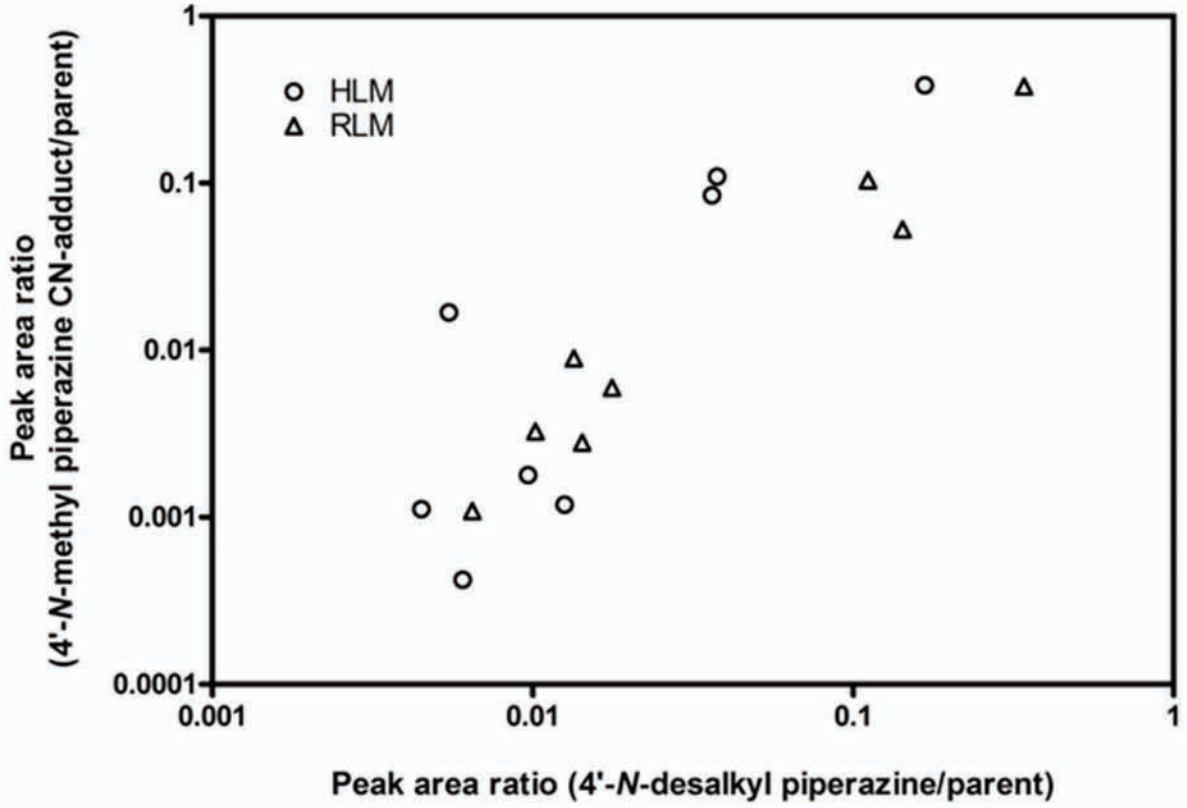

Figure 15

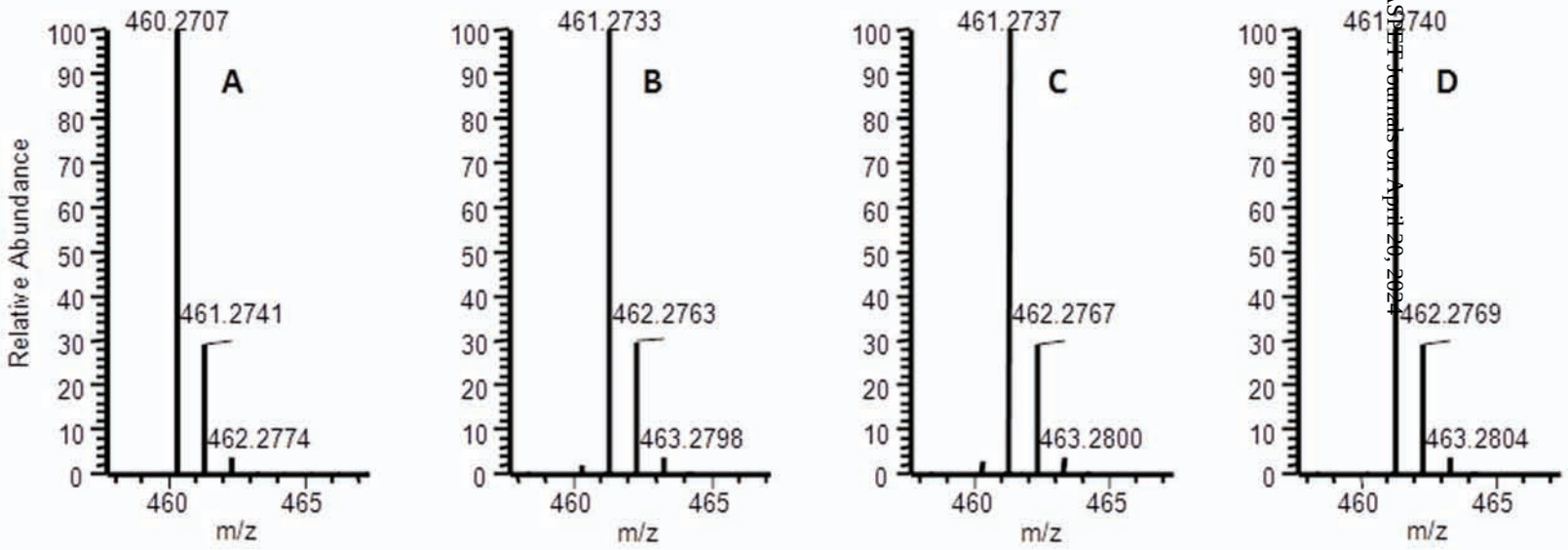

Figure 16

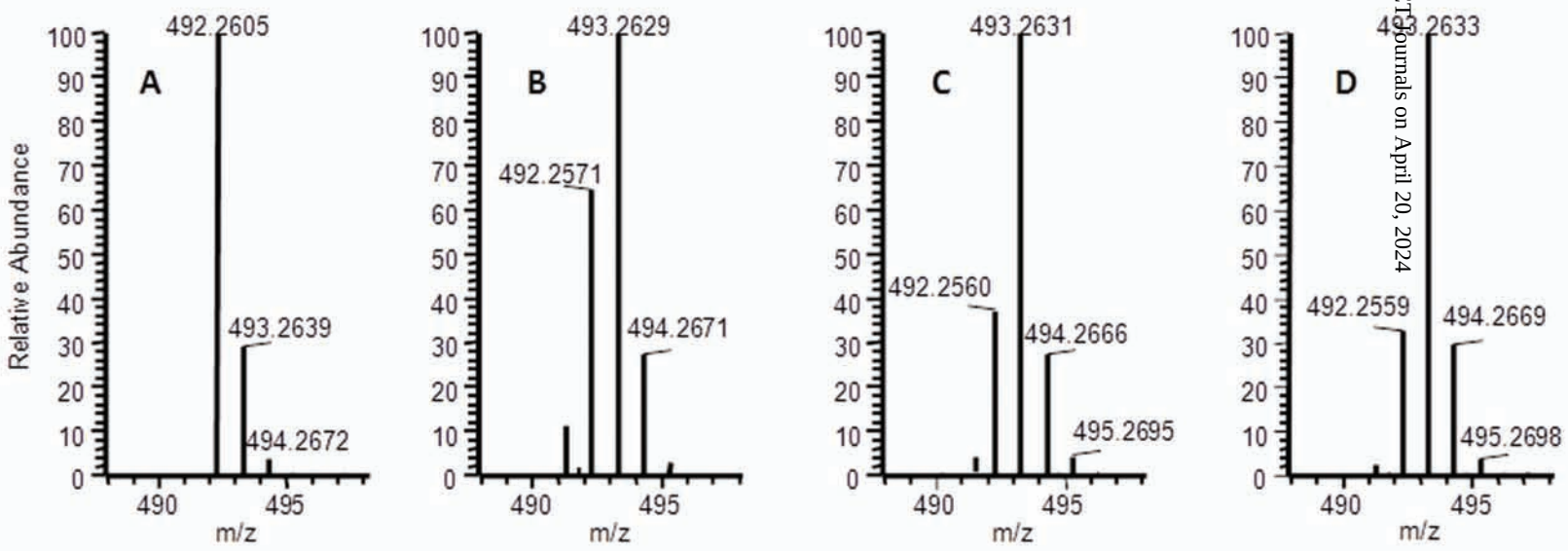

Figure 17

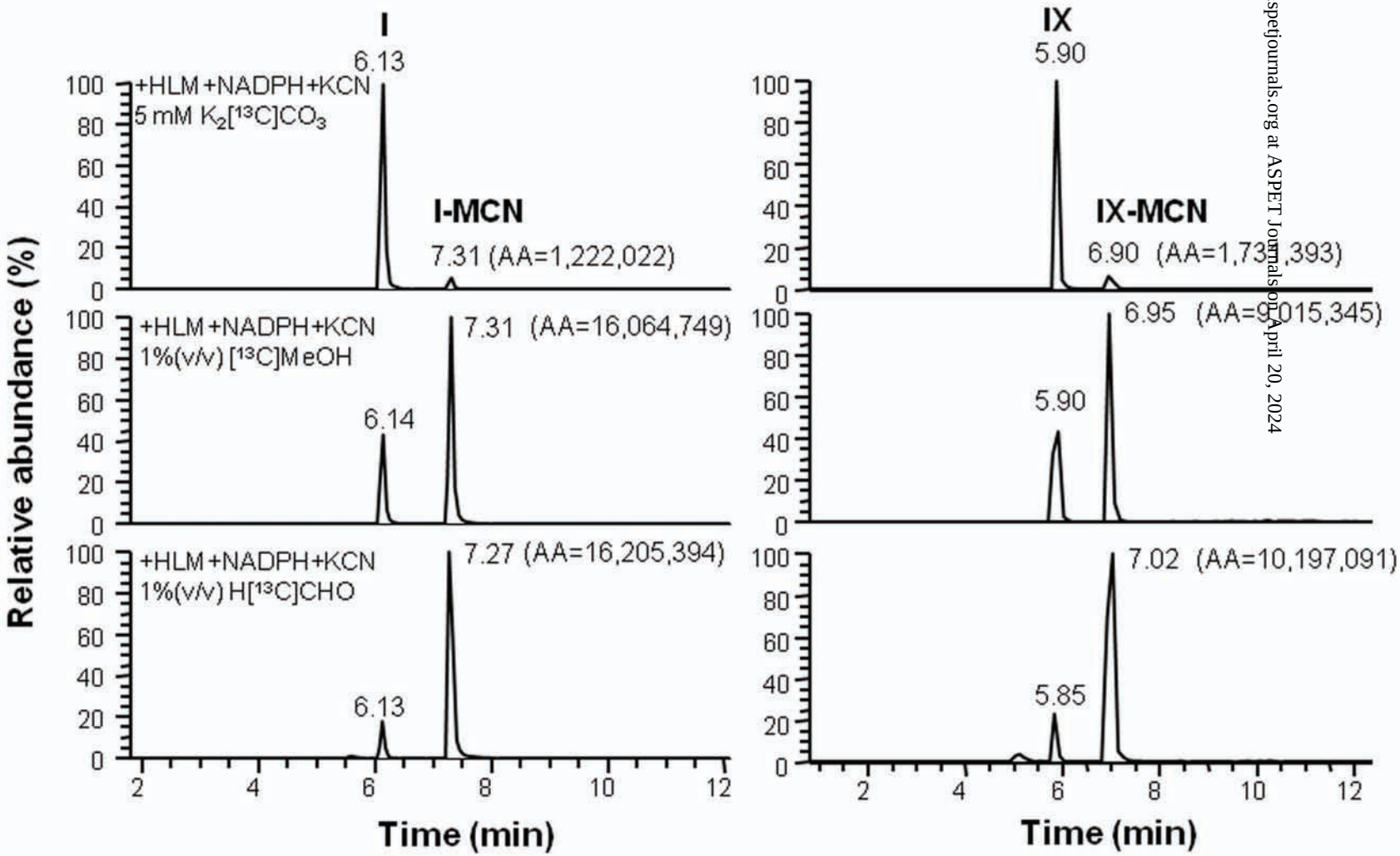

Figure 18

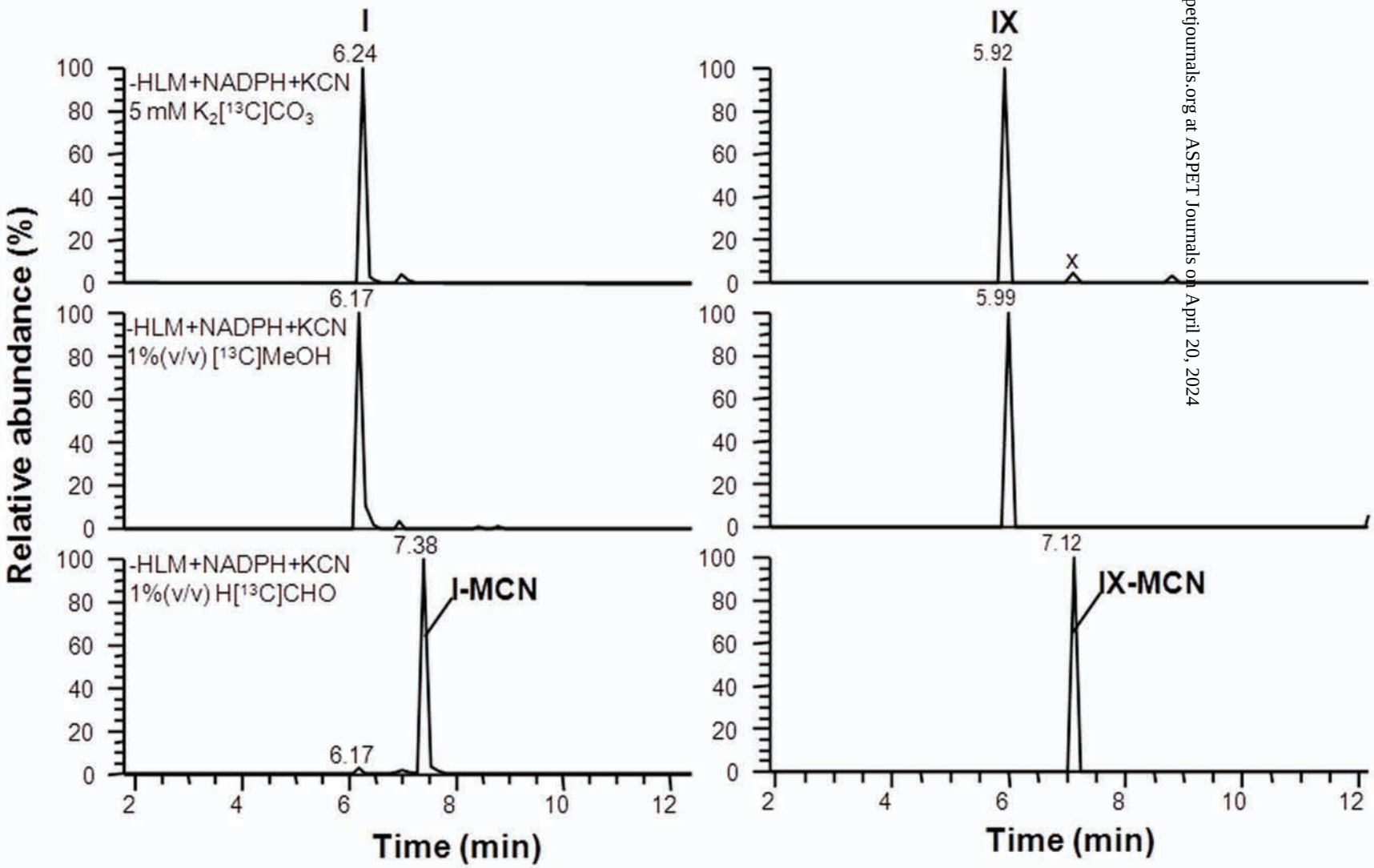

Figure 19

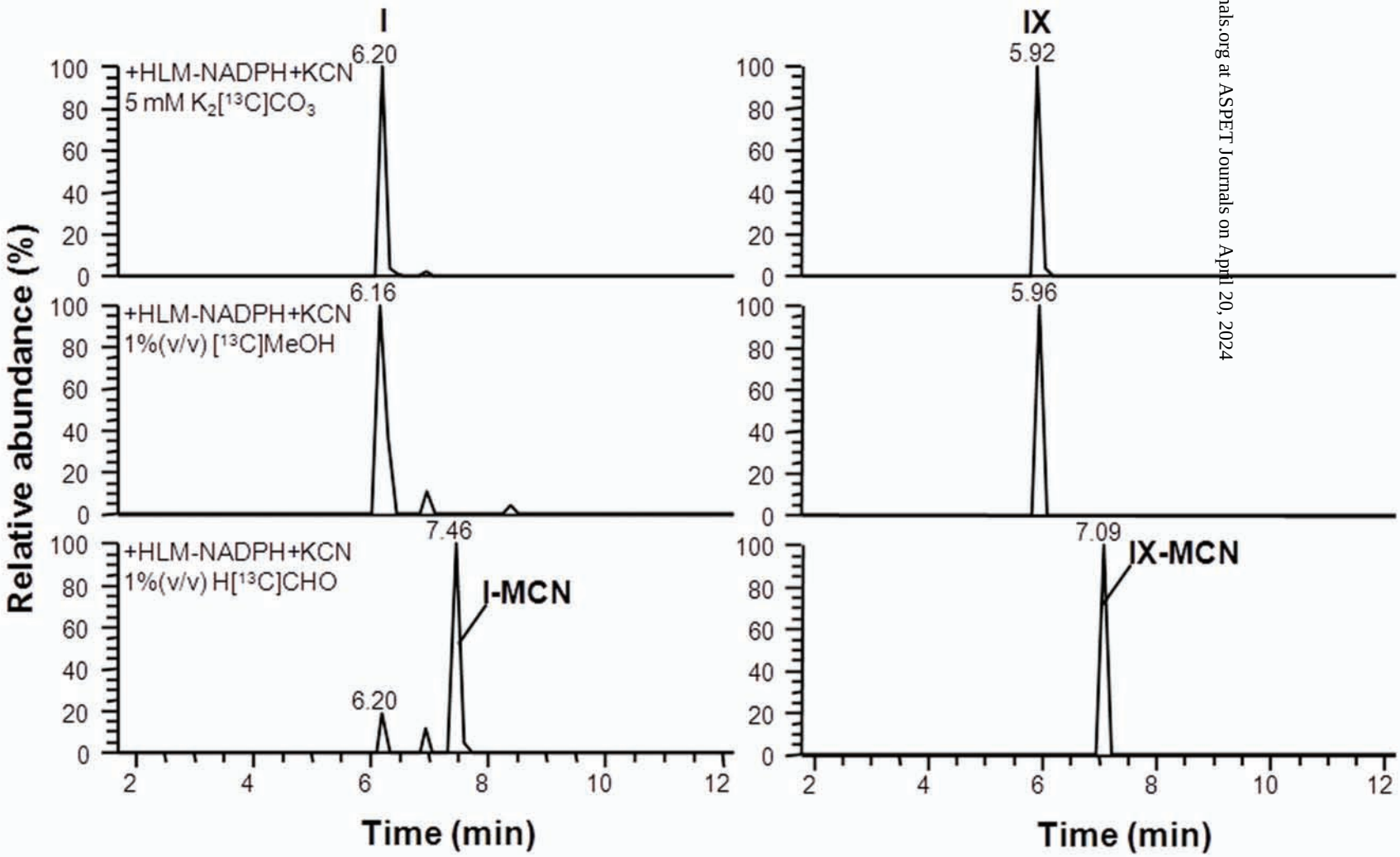

Figure 20